ADVANCED ENERGY MATERIALS
www.advenergymat.de

Conversion of Methane into Liquid Fuels—Bridging Thermal Catalysis with Electrocatalysis

Shuai Yuan, Yanding Li, Jiayu Peng, Ydna M. Questell-Santiago, Karthik Akkiraju, Livia Giordano, Daniel J. Zheng, Sujay Bagi, Yuriy Román-Leshkov, and Yang Shao-Horn**

The direct partial oxidation of methane to methanol promises an energy-efficient and environmental-friendly utilization of natural gas. Unfortunately, current technologies confront a grand challenge in catalysis, particularly in the context of distributed sources. Research has been focused on the design of homogenous and heterogenous catalysts to improve the activation of methane under thermal and electrochemical conditions. However, the intrinsic relationship between thermal and electrochemical systems has not been exploited yet. This review intends to bridge the studies of thermal and electrochemical catalysts, in both homogenous and heterogenous systems, for methane activation from a mechanistic point of view. It is expected to provide a framework to rationalize the design of electrocatalysts beyond the state of art. First, methane activation systems reported previously are reviewed and classified into two basic mechanisms: dehydrogenation and deprotonation. Based on the mechanism types, activity and selectivity descriptors are defined to understand the performance of current catalysts and guide the design of future catalysts. Moreover, methods to enhance the activity and selectivity are discussed to emphasize the unique advantage of electrocatalysis in overcoming the limitations of traditional thermal catalysis. Finally, immense opportunities and challenges for catalyst design are discussed by unifying thermal and electrochemical catalysis.

1. Introduction

As the main component of natural gas, methane is a well-established and widely available feedstock to produce several important commodity chemicals including methanol, hydrogen, ammonia, and formaldehyde.[1] With the recent discoveries of vast shale gas reserves, the energy landscape of the United States is shifting toward an increased prominence of natural gas in the feedstock portfolio.[2] Despite being widely deployed, methane conversion processes are bound by the intrinsic chemical inertness of its C—H bonds.[3] For example, liquid fuel production from methane can be accomplished through steam reforming followed by Fischer–Tropsch synthesis (**Figure 1**a).[4] Steam-methane reforming ($CH_4 + H_2O \rightleftharpoons CO + 3\ H_2$) is an endothermic (≈200 kJ mol^{-1}) process requiring elevated temperatures (700–1100 °C) and is typically catalyzed by alumina-supported nickel catalysts.[4] Although lowering the pressure increases the thermodynamic driving force of steam-methane reforming reaction, high pressures (typically above 10 bar) are usually applied to accelerate the reaction.[4] Industrially, the thermal energy requirement for this reaction is typically met through the combustion of methane, which effectively lowers the feedstock efficiency of the process. Indeed, about 25–35% of the total methane feed is burned for heat[5] instead of producing the desired syngas product as a feedstock of subsequent Fischer–Tropsch synthesis. Furthermore, a large number of unit operations and centralized infrastructure are required to accommodate the circuitous energetic pathways, thus hindering their implementation on a small scale. For this reason, at remote oil fields lacking the infrastructure to store, transport, or utilize the produced natural gas, methane is typically burned as flare gas, resulting in a total waste of 140 billion m^3 methane every year, equivalent to a market cost of ≈$20 billion per year.[6] To address this problem, an attractive solution is to convert methane to liquid fuels, such as methanol, via selective partial oxidation using existing infrastructure that can be easily deployed and mobilized in remote oil fields.[7] Such methane-to-liquid fuels technology will significantly improve the volumetric energy

Dr. S. Yuan, Prof. L. Giordano
Research Laboratory of Electronics
Massachusetts Institute of Technology
Cambridge, MA 02139, USA
Dr. S. Yuan, Dr. Y. Li, Dr. Y. M. Questell-Santiago, S. Bagi, Prof. Y. Román-Leshkov
Department of Chemical Engineering
Massachusetts Institute of Technology
Cambridge, MA 02139, USA
E-mail: yroman@mit.edu
Dr. S. Yuan, J. Peng, K. Akkiraju, D. J. Zheng, Prof. Y. Shao-Horn
Department of Materials Science and Engineering
Massachusetts Institute of Technology
Cambridge, MA 02139, USA
E-mail: shaohorn@mit.edu
Prof. L. Giordano, S. Bagi, Prof. Y. Shao-Horn
Department of Mechanical Engineering
Massachusetts Institute of Technology
Cambridge, MA 02139, USA
The ORCID identification number(s) for the author(s) of this article can be found under https://doi.org/10.1002/aenm.202002154.

DOI: 10.1002/aenm.202002154

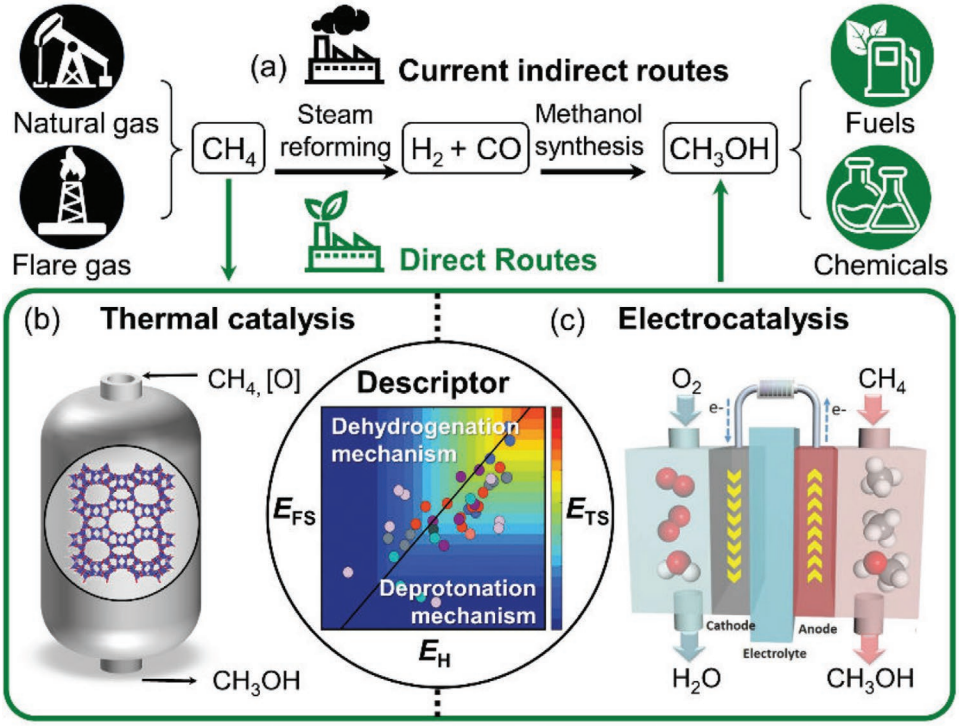

Figure 1. Chemical pathways to produce methanol from a) conventional two-step steam reforming as centralized and energy-intensive routes, and b) direct routes by thermal catalysis and c) electrocatalysis. Inset shows the intrinsic similarity of thermal catalysis and electrocatalysis in the reaction mechanisms and activity descriptors. Descriptor plot adapted with permission.[22] Copyright 2017, Royal Society of Chemistry.

density of methane (0.0378 MJ L^{-1} for methane and 17.8 MJ L^{-1} for methanol at 1 bar, 15 °C),[8] therefore reducing the transportation cost by gas pipeline, cryogenic liquefied natural gas tanks, or high-pressure compressed natural gas cylinders.

The challenges of selective methane partial oxidation stem from the lower reactivity of methane molecules compared to that of its oxidation products. The reactivity differences between methane and methanol can be understood by comparing their homolytic bond dissociation energies (BDE) and pK_a values. The BDE of methane is 440 kJ mol^{-1}, which is higher than that of methanol (400 kJ mol^{-1}). This implicates a more difficult dehydrogenation (H-abstraction) reaction for methane than methanol.[9] The symmetric tetrahedral geometry of methane molecules and the weakly polarized C–H bonds result in extremely weak acidity (pK_a of 40 for methane and 15 for methanol), making methane more resistant to deprotonation reactions.[9] Other physical/chemical properties quantified by the electron affinity (activation by nucleophiles), proton affinity (activation by protons), and ionization potential (activation by removal of electrons) all predict higher stability of methane compared to methanol, **Table 1**.[9] The reactivity estimation of methane and methanol by BDE and pK_a is based on the assumption that the energetics in activating C–H bonds by deprotonation or dehydrogenation scale with activation barriers for all elementary reaction steps.[10] While methane can readily dissociate on the catalyst surface (e.g., Ni—CeO_2[11] and IrO_2[12]), the adsorption energetics of dissociated species (*CH_3) correlated by BDE and pK_a can govern the energetics of further bond breaking/making to form intermediates (*CH_2OH, etc.). In support of this assumption, there is a constant difference of ≈40 kJ mol^{-1} between the dehydrogenation activation energies of methane and methanol across a wide range of catalysts, which is comparable with the difference in BDE.

Over several decades, research efforts focused on direct methane partial oxidation have not yet generated a viable industrial process.[13–18] The thermal catalysis of methane partial oxidation has been explored using metals, metal complexes, metal oxides, and metal-exchanged zeolites bearing transition metal centers including Cu, Fe, V, Ir, Pd, Pt, Rh, etc. (Figure 1b).[13] Unfortunately, these catalytic reactions usually require either strong oxidants (e.g., N_2O and H_2O_2)[14–18] or high thermal energy (when O_2 is used as the oxidant)[19,20] to overcome the energy barrier for C–H bond activation or active site regeneration. The latter conditions often result in the overoxidation of methanol to the thermodynamically more favorable product, CO_2. For this reason, high selectivity to desirable products can only be achieved at low conversions.[13,21,22]

Electrocatalysis has shown unique advantages to realize an efficient and selective methane partial oxidation process by overcoming key limitations of the thermal systems (Figure 1c).[23–27] Electrochemical methods enable the control of the chemical potential of the catalyst surface,[28,29] facilitating operations at low temperatures (<100 °C). Accordingly, this approach could avoid the use of strong oxidants (N_2O, H_2O_2) and high thermal energy requirements needed to activate methane and/or regenerate active sites. The driving force for methane oxidation can be systemically tuned by varying the electrode potential, which may lead to a nonequilibrium population of highly reactive

Table 1. Comparison of physical/chemical parameters for methane and methanol.[9]

	BDE [kJ mol^{-1}]	pK_a	Electron affinity [kJ mol^{-1}]	Proton affinity [kJ mol^{-1}]	Ionization energy [kJ mol^{-1}]
CH_4	440	40	145	552	1215
CH_3OH	400	15	135	761	1042

metal centers[30] and thus to faster reaction rates than those of thermal processes. Meanwhile, the mild reaction conditions at room temperature may avoid the overoxidation of methanol.[27] The electricity requirement to drive methane electrocatalysis can be supplied by renewable energy resources, such as solar energy or wind power, to achieve sustainable methanol production.[31] In addition, with efficient electrocatalysts, a fuel-cell-like reactor operated at low overpotential could be designed to produce electricity as a byproduct of fuel production.[32–35] In principle, such a device could generate energy in the form of electricity rather than consuming energy, while producing methanol as a liquid fuel. More importantly, electrochemical devices are highly modular,[36] because the productivity scales directly with electrode size and current, thus providing an efficient and cost-effective solution that can be deployed in both large-scale industries and small-scale applications (such as those needed in remote oil fields).[37] Despite all of these merits, several challenges remain in the design of electrochemical systems that are financially competitive with current industries (i.e., steam reforming and Fischer–Tropsch synthesis). A detailed techno-economic analysis of a methane-to-methanol fuel cell system identified the minimum required performance metrics for the economic viability of the process, namely, 70% methanol selectivity and ≈0.5 V cell potential (i.e., ≈1 V overpotential) at a current density of 100 mA cm^{-2} in the temperature range of 100–250 °C.[37] Current electrocatalysts are inadequate to make the electrochemical scheme practical. The key challenge to meet this requirement is the development of selective electrocatalysts to convert methane into methanol at a lower overpotential and a higher current.

Researchers have been working on the electrocatalytic methane activation over six decades, leading to the discovery of various electrocatalysts and relevant devices. These electrocatalysts and electrochemical devices have been summarized in several comprehensive reviews.[8,23–27,38] However, it still lacks a review to mechanistically rationalize current electrocatalysts and guide the design of future electrocatalysts for methane activation. This review article intends to bridge the studies of thermal and electrochemical catalysts in both homogenous and heterogenous systems for methane partial oxidation, with the ultimate goal of providing a robust framework to understand the performances of current catalysts and provide guidance in the design of future catalysts. First, we evaluate current methane activation systems and categorized them into two basic mechanisms, dehydrogenation and deprotonation. Next, we define fundamental activity and selectivity descriptors based on each mechanism. In this context, we discuss past and present thermal and electrochemical methane oxidation catalysts in homogenous and heterogenous systems with a special focus on recent studies on the mechanistic understanding of Fe- and Cu-zeolite catalysts, as well as single-atom catalysts based on zeolites, oxides, and graphene. We rationalize the design and performance of these catalysts emphasizing their limitations in C–H activation, active-site regeneration, and selectivity. Finally, we discuss the opportunities of electrochemistry in the design of future electrocatalysts with enhanced activity and selectivity guided by the activity/selectivity descriptors to overcome the inherent limitations of current catalysts.

2. Reaction Mechanisms for the Partial Oxidation of Methane

2.1. Current Understanding of Methane Partial Oxidation

A multitude of catalysts and catalytic systems for partial methane oxidation with various oxidants have been reported over a century. Early reports used VO_x and MoO_x to oxidize methane with O_2 at high temperatures (e.g., 450 °C) to produce formaldehyde as the main product and methanol as a side product (yields of ≈3–4% and formaldehyde selectivity of 30–70%).[39] More recently, metal exchanged zeolites with Cu- and Fe-metal centers have attracted increasing interest due to their ability to readily activate C—H bonds at mild conditions either stoichiometrically or catalytically.[19,40] Specifically, activated M–O sites within these catalysts have been shown to oxidize C–H bonds at temperatures as low as 150 °C with O_2 or at room temperature with H_2O_2.[40] However, the regeneration of active M–O sites by O_2 usually requires high temperature (>400 °C) whereas strong oxidants (such as H_2O_2) are needed for active site regeneration at room temperature.[40] To avoid the overoxidation of methanol at high temperatures, a stepwise process is used to achieve an over 90% methanol selectivity. In this process, Cu-zeolite is first activated in O_2 at 450 °C and then cooled to 200 °C to react with methane in the absence of oxygen.[19] Continuous methanol production can be realized using O_2 as the sole oxidant over the same Cu-zeolites, but a trade-off exists between the conversion and selectivity (<0.01% conversion to maintain 70% selectivity).[41] Metal nanoparticles and metal complexes with Pt and Pd centers have been explored for C–H bond activation, as exemplified by the Periana's system which uses Pt^{2+}-complex-based catalysts in concentrated sulfuric acid (H_2SO_4).[42] The H_2SO_4 not only acts as an oxidant but also stabilizes the methyl bisulfate product, achieving an impressive ≈90% conversion and 81% selectivity. However, the nonrecyclable H_2SO_4 oxidant and the water-sensitive catalytic center hinder the practical application of this system. Electrochemical methane partial oxidation stems from the study of methane fuel cells using Pt and Pd as anode catalysts with CO_2 as the main product.[26] Later on, V_2O_5 has been used as the anode catalyst to achieve high methanol selectivity (88%).[43,44] Other thermal catalysts such as Pt, Pd, and their complexes have also been applied in electrocatalytic systems, where oxidants or high-valent active sites can be regenerated electrochemically.[30]

Besides the diverse compositions of these catalysts, a variety of reaction mechanisms have been proposed for different catalysts, which makes it difficult to define a universal activity descriptor across these materials. For homogenous catalysts,

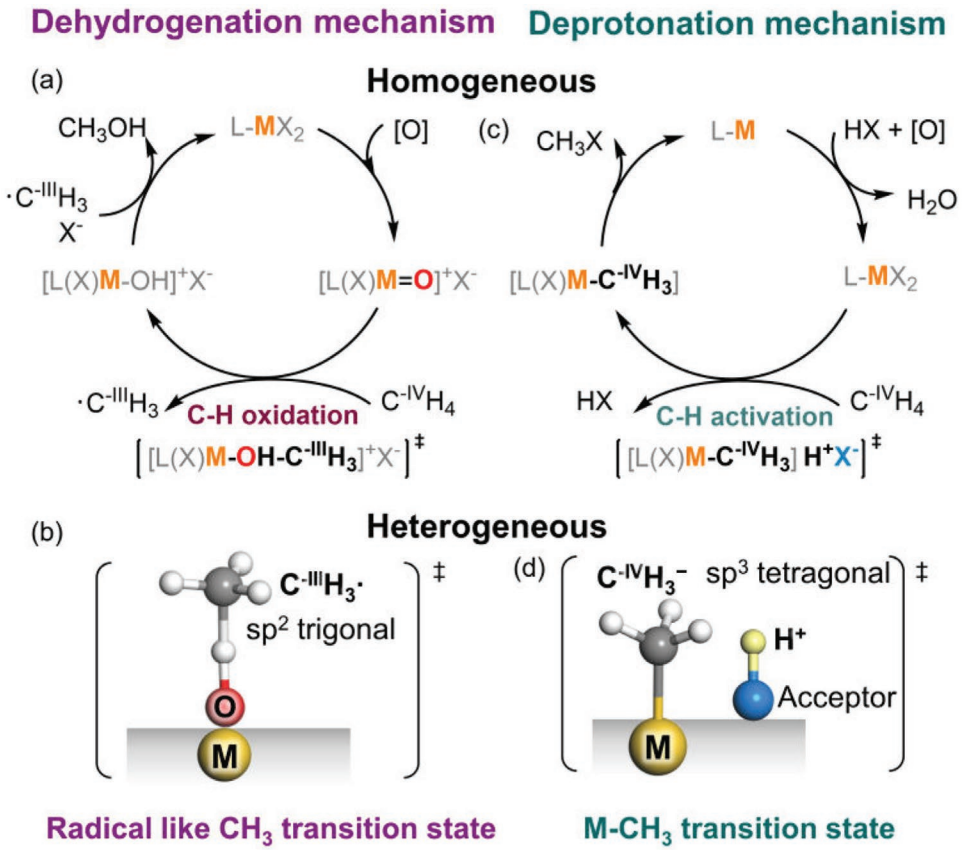

Figure 2. Two mechanisms of methane activation for homogenous[9] and heterogenous catalysis.[55] The dehydrogenation mechanism corresponds to a) the C—H oxidation in homogenous catalysis and b) radical pathway in heterogenous catalysis. The deprotonation mechanism corresponds to c) C—H activation in homogenous catalysis and d) surface-stabilized M—CH_3 pathway in heterogenous catalysis. M, L, X, and [O] represents metal centers, neutral ligands, anionic ligands, and oxidants, respectively.

the C–H activation mechanisms at metal centers have been proposed to occur through oxidative addition, electrophilic activation, σ-bond metathesis, metalloradical activation, and 1,2-addition depending on the metal centers.[45] For example, the oxidative addition mechanism has been proposed for low-valent late transition metal complexes with electron-rich metal centers (e.g., Ru, Os, Rh, Ir, and Pt). Electrophilic activation is commonly observed in late- or post-transition metals complexes (Pd^{2+}, Pt^{2+}, Hg^{2+}, Tl^{3+}) in strong polar solvents (e.g., H_2O, H_2SO_4). Early-transition metal centers with d^0 electronic configurations (e.g., Sc^{3+}, lanthanides) and alkyl ligands have been reported to undergo σ-bond metathesis in which an alkyl ligand on metals is replaced by a methyl group from methane. For heterogenous catalysts, the •CH_3 radical and the surface stabilized M–CH_3 have been proposed as transition states of different materials.[8] A unified understanding of reaction mechanisms is needed to predict the activity trend and guide the design of future catalysts.

2.2. Unifying the Mechanisms for Methane Activation

The dissociation of a C—H bond in methane is a critical step in methane oxidation. Note that the difference between thermal and electrochemical systems lies in the generation of active sites, which can be procured either by an oxidant at thermochemical conditions or an anodic potential. The reaction mechanisms of C–H dissociation of methane can be classified into two categories: dehydrogenation and deprotonation. Different nominations have been used in the discussion of these two mechanisms in homogenous (C—H oxidation and C—H activation pathways)[9] and heterogenous systems (radical and surface-stabilized M—CH_3 pathways),[46] but for all purposes, they can be lumped under one of these two mechanisms based on the fundamental nature of the reaction pathways (**Figure 2**).

The dehydrogenation mechanism involves an abstraction of a hydrogen atom (•H) from CH_4 by active electrophilic oxygen atoms (such as heterogenous M—O sites or homogenous metal-oxo complexes) to form •CH_3 and •OH radicals in the transition state.[47] The •CH_3 radicals weakly interact with the catalytic center through •OH sites without forming M—C bonds. The carbon center has a formal oxidation state (FOS) of –III (Figure 2a) and sp^2 hybridization, showing a geometry close to trigonal (Figure 2b). This mechanism is terminated as a C—H oxidation step in the discussion of homogenous catalysts because of the increased FOS of C from –IV to –III in the generation of the reaction intermediate.

The deprotonation mechanism initiates by the dissociative adsorption of CH_4 to generate CH_3^- and H^+.[9,22,45] On the one hand, the CH_3^- concomitantly coordinates to the catalyst surface

to form an M−C σ-bond. On the other hand, the H^+ can be accepted by the surface metal, surface O species (heterogenous catalysts), ligands, or molecules in solution (homogenous catalysts). More specifically, the M−C σ-bonds can be formed by σ-bond metathesis, oxidative addition, or electrophilic activation depending on the nature of the metal center.[9,45,48] In all cases, the carbon center maintains an FOS of –IV (Figure 2c) and shows a tetrahedral geometry with sp^3 hybridization (Figure 2d). This deprotonation mechanism is also referred to as the "C−H activation mechanism"[9] in the discussion of homogenous catalysts because there is no change in the FOS of carbon in the generation of the reaction intermediate. Unlike the radical mechanism, in which the $\bullet CH_3$ radical weakly interacts with the catalyst surface, the CH_3^- motif is stabilized by forming an M−CH_3 σ-bond. Therefore, the M−CH_3 transition states are also termed as "surface-stabilized transition states"[22] in the discussion of heterogenous catalysts. The deprotonation mechanism implies that the methane activation step is an acid–base reaction without FOS change of the carbon center. It agrees with the observation that the deprotonation mechanism often occurs in the homogenous systems of highly polar solvents, such as water or anhydrous acids (e.g., H_2SO_4).[9] Density functional theory (DFT) calculations of actual electronic distribution generally show little changes in electronic distribution and geometry of the carbon atom in the transition states of Pt−CH_3 and Pd−CH_3 for deprotonation mechanisms, which confirms the assignment of the FOS.[49–51]

The catalytically active oxygen species can be electrophilic or nucleophilic.[52] Electrophilic oxygens are electron-deficient species (e.g., O^-, O_2^-) usually formed by the strong oxidants (e.g., O_2, N_2O), which promote the dehydrogenation of C−H bonds. On the other hand, nucleophilic oxygens are electron saturated species (O^{2-}), which often act as H^+ acceptors and catalyze the deprotonation of C−H bonds.[53] Therefore, the dehydrogenation mechanism is generally observed for strong oxidizing catalysts (e.g., high-valent metal-oxo species such as Fe^{IV}−O[54]). In contrast, the deprotonation mechanism usually occurs on metals or metal complexes with low oxidation states metal centers (such as Pt and Pt^{II} complexes) and accessible H^+ acceptors.[42] Accurate determination of the C−H activation mechanism requires the comparison of transition state energy (E_{TS}) by two pathways, which will be discussed in the following section.

In addition to the dehydrogenation and deprotonation mechanisms, some methane oxidation reactions are initiated by free radicals, sometimes accompanied by promoters to generate radicals (such as Fe^{2+} in the Fenton reaction to generate $\bullet OH$).[56] Similarly, plasma has been used to convert methane and oxygen into partially oxidized C_1 species.[57] As the transition states of C−H cleavage in these systems are largely independent of the "catalytic" metal centers, they will not be discussed in this review. The reaction mechanisms in Figure 2 only depict the methane-to-methanol conversion pathway and omit the side reactions for clarity. Considering all the possible side products (H_2, CH_2O, HCOOH, C, CO, and CO_2) and intermediates (*CH_3, *CH_2OH, *CH_2O, *CHO, and *COOH), the methane partial oxidation process can be described by a more complex reaction network (Figure S1, Supporting Information).[58,59] The precise identification of reaction mechanisms, the rate-limiting step, and reaction kinetics within the reaction network usually requires a combination of catalytic experiment, in situ characterization, and kinetic modeling.[58,59] To establish a simple model for the study of activity and selectivity trends over a wide range of catalysts, herein, only the methane-to-methanol pathway is considered. Detailed reaction path analyses and microkinetic modeling of methane oxidation kinetics on different catalytic systems, such as Ni and PdO, have been well-demonstrated by Deutschmann and others in a series of comprehensive studies,[58–63] and will not be discussed in this review.

3. Descriptors and Design Principles for Methane Partial Oxidation Catalysts

3.1. Activity Descriptors

Researchers have been devoted to developing universal activity descriptors that can correlate the experimental activity (or computed transition state barrier) with more accessible parameters, such as the energy of key adsorbates or the final state of an elementary step. Activity descriptors allow the rough prediction of catalytic activity before performing large-scale catalytic tests or expensive activation barrier computations, which accelerates the rational design of catalysts and reaction screening.[64,65] Fundamentally, activity descriptors are established based on linear energy scaling relationships of transition states and intermediates.[66] As methane activation undergoes two pathways with different transition states, distinct energy scaling behaviors are expected that will lead to different activity descriptors. In the dehydrogenation mechanism that proceeds through a radical-like transition state, methane activation transition state energies (E_{TS}) scale with the hydrogen affinity (E_H) of the active site. In the deprotonation mechanism that proceeds through the M−CH_3 transition states, the E_{TS} scales with the final state energy of deprotonation (E_{FS}), whereas E_{FS} is governed by the binding energy of both –H and –CH_3 to the surface.

3.1.1. Activity Descriptor for the Dehydrogenation Mechanism

For this mechanism, we consider two elementary steps for methane activation: the (re)generation of active sites by O_2 (M + $0.5O_2$ → M–O) and the breaking of C−H bonds (M–O + CH_4 → M–OH + $\bullet CH_3$). Hydrogen affinity or hydrogen adsorption energy (E_H), defined as the energy difference between hydrogenated and bare active sites, is an activity descriptor for C−H bond activation on transition metal oxides that undergoes radical-like transition states.[67,68] Nørskov and co-workers further demonstrated that E_H is a universal descriptor for predicting C−H activation barriers of methane over a wide range of catalysts that proceed via similar radical transition states.[69] Their calculations covered certain types of metals, metal oxides, metal-exchanged zeolites, metal–organic frameworks (MOFs), and metal-embedded graphene. A linear scaling relationship was observed between the calculated E_{TS} and E_H, indicating that electron-deficient metal centers with low E_H tend to stabilize the radical transition state and thus increase the catalytic activity per active site (**Figure 3**a).

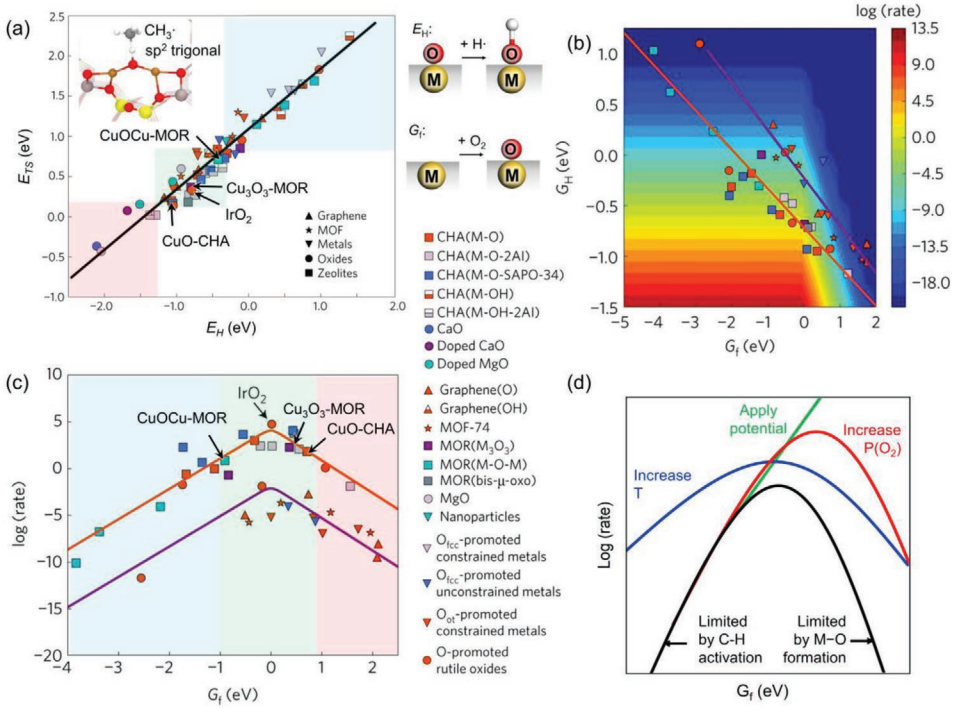

Figure 3. Activity descriptor for methane activation by dehydrogenation mechanism. a) Universal scaling relationship between transition state energy (E_{TS}) and hydrogen affinity (E_H). The left inset illustrates the TS geometry for a representative catalytic center of CuOCu-MOR. The right inset shows scheme representation of E_H and active site formation free energy (G_f). b) 2D volcano plot as a function of hydrogen adsorption-free energy (G_H) and G_f. Blue, green, and red shaded areas represent strong, medium, and weak oxygen binding, respectively. c) 1D volcano plot using G_f as the descriptor. d) Correlation between computed reaction rate and G_f obtained from Equation (1) (black) assuming a linear correlation between activation free energy (ΔG_a) and G_f to show the effect of temperature (blue), O_2 pressure (red), and potential (green) on the reaction rate. Reproduced with permission.[69] Copyright 2017, Springer Nature.

While E_{TS} reflects the activity per active site (M−O site), the active site coverage (ϑ_{motif}) is governed by the formation energy of active M−O sites (G_f). By combining the activation energy predicted from E_H with the active site coverage derived from G_f, the reaction rate for methane activation (M + 0.5O_2 + CH_4 → M−OH + •CH_3) can be calculated using Equation (1), which involves the formation of active sites (M + 0.5O_2 → M−O) and the activation of methane (M−O + CH_4 → M−OH + •CH_3) as two elementary steps (Figure 3b). A linear correlation between E_H and G_f descriptors was observed. Therefore, a rate-based volcano plot (Figure 3c) can be established by further considering the observed linear correlation between E_H and G_f, thus illustrating the correlation between the C−H activation rate and G_f (or E_H). Materials at the left branch of the volcano plot are limited by the active site coverage (i.e., high formation energy of M−O sites), while materials on the right side are limited by high C−H activation barriers. Materials at the peak of the volcano are the most promising methane oxidation catalysts, as they are likely to have the optimal balance between C–H activation rates and active-site coverage. The most active methane oxidation catalysts predicted by this analysis, including IrO_2[12] and Cu-exchanged zeolites (Cu-O-Cu/MOR,[70] bis-μ-oxo-Cu/MOR,[19] and Cu_3O_3/MOR[71]), have been experimentally demonstrated as effective catalysts for methane activation. Recently, this method has been successfully applied to screen MOF-based catalysts for methane oxidation, which possess more diverse structures, compositions, and metal coordination environments than traditional oxides and zeolites[72]

$$\text{Rate} = \theta_{\text{motif}} \frac{k_B T}{h} \exp\left(\frac{-\Delta G_a}{k_B T}\right) = \frac{\sqrt{P_{O_2}}\, e^{-G_f/k_B T}}{1+\sqrt{P_{O_2}}\, e^{-G_f/k_B T}} \frac{k_B T}{h} \exp\left(\frac{-\Delta G_a}{k_B T}\right) \quad (1)$$

The effect of different reaction conditions on the reaction rate of methane activation can be predicted using Equation (1). Assuming that the hydrogen activation free energy (ΔG_a) and G_f are linearly correlated, an increase in reaction temperature increases the reaction rate while broadening the volcano curve (Figure 3d). The peak position of the volcano plot shifts slightly to stronger oxygen-binding materials with lower G_f values. Increasing the O_2 pressure or using strong oxidants, such as N_2O, increases the activity for the materials that bind oxygen weakly, effectively shifting the volcano peak to materials with higher G_f. For the right branch of the volcano plot, where the reaction rate is thermodynamically limited by the formation of M–O active site, the application of electrochemical potentials to generate active sites should improve the reaction rate by overcoming this limitation. This limitation is also seen in many reaction rates in thermal catalysts which are restricted by the (re)generation of active sites by O_2. For example, the (re)generation of active Cu–O species in Cu-exchanged zeolites by O_2 requires at least 400 °C, whereas the subsequent C–H breaking can proceed at 200 °C.[19]

Rossmeisl and co-workers have investigated the electrochemical process of methane partial oxidation by considering an electrochemical formation of surface M–O moieties and a subsequent thermal catalytic methane activation by these M–O species.[29] These authors revealed a linear relationship between methane activation energy and oxygen binding energy on the surface (E_O). As oxygen binding energies have been widely applied in predicting the activity of electrocatalysts for oxygen evolution reaction (OER)[73,74] and oxygen reduction reaction (ORR),[73–75] the E_O descriptor will facilitate the discovery of methane oxidation catalysts based on current OER and ORR catalysts. Indeed, the E_O and G_f descriptors are intrinsically related, as they both describe the formation energy of surface M–O active sites; it is expected that strong oxygen-binding materials will have low E_O and G_f and vice versa. Other activity descriptors such as oxygen vacancy formation energy have also been proposed to predict the methane activation trend on oxide catalysts.[76]

3.1.2. Activity Descriptor for the Deprotonation Mechanism

Some transition metals, such as Pd, Pt, and Rh, lie out of the linear E_{TS}–E_H scaling relationship because they are capable of stabilizing the methyl group and instead follow the deprotonation mechanism.[22,77] The transition state of the deprotonation mechanism involves the deprotonation of CH_4 and the binding of both CH_3^- and H^+ to the surface ($M + X + CH_4 \rightarrow M–CH_3 + H\text{-}X$ where M stands for metal sites and X represents H^+ acceptor). The transition state can be predicted by the Brønsted–Evans–Polanyi relationship,[10,77–80] wherein E_{TS} scales with the final state energy of deprotonation (E_{FS}) and E_{FS} is determined by the binding energy of CH_3^- and H^+ to the surface (**Figure 4**a).[22] The E_{TS}–E_{FS} scaling relationship has been demonstrated for several oxides, metals, oxygen promoted metals, and sulfides (Figure 4c). The E_{FS} descriptor predicts that noble metals, such as Pt, Pd, and Rh, are viable catalysts for methane activation due to their low E_{TS}, in agreement with experimental results in the literature.[81,82] The transition state can be stabilized by suitable acceptors (Figure 4b) such as surface metals, surface oxygens, lattice oxygens, and ligands. For example, ligands or solvents around metal centers have been proposed to act as H^+ acceptors, as proposed in Pt^{2+}-H_2SO_4 homogenous catalytic systems.[83] Nørskov and co-workers have shown that oxygen promoted metals generally have lower E_{TS} compared to the bare metal surface[22] due to the stabilization of H^+ by oxygen acceptors. Although oxygen coverages on these noble metals are expected to be low considering their unfavorable formation energies, oxygen-promoted Au and Ag have nearly the same E_{TS} compared to bare Pt and Pd which are known as active methane oxidation catalysts.[84] In this respect, using electrocatalytic methods may promote the formation of surface-oxidized M−O species as acceptors thus enhancing the overall reaction rate.

Estimation of C−H activation barriers by a suitable descriptor requires the proper determination of the reaction mechanism. Nørskov and co-workers calculated E_{TS} based on both dehydrogenation and deprotonation mechanisms, and define that the lower one of two descriptors can represent E_{TS} more accurately. They further compared the E_{TS} as a function of two descriptors E_H and E_{FS} (Figure 4d).[22] The trendline, defined by the equation of $E_{FS} = 1.12E_H + 0.07$, indicates two descriptors predicting equal E_{TS}. Materials above the trendline ($E_{FS} > 1.12E_H + 0.07$, i.e., materials with high E_{FS} and low E_H) generally undergo a dehydrogenation pathway, whereas materials below the trendline ($E_{FS} < 1.12E_H + 0.07$, i.e., materials with high E_H and low E_{FS}) may follow a deprotonation pathway or dehydrogenation pathway depending on the geometry of catalytic centers. The deprotonation pathway is more likely in the presence of acid–base pairs or accessible acceptors. For instance, the active sites in zeolites are spatially separated, which prohibits the deprotonation pathway regardless of $\bullet CH_3$ binding favorability. IrO_2 (110) has a radical-like TS possibly due to the segregated •OH and $\bullet CH_3$ binding sites, even though the energetic analysis would predict the methyl group to be surface-stabilized. The deprotonation mechanism is commonly observed for homogenous catalysts in highly polar media, where metals exist in low oxidation states and proton acceptors are easily accessible. By defining the proper reaction mechanism and activity descriptor, this model can be used to quickly estimate transition state energies of methane activation over a wide range of catalysts.

Fundamentally, the descriptors, such as E_H, G_f, E_O, and E_{FS}, are all governed by the intrinsic electronic structures and properties of materials. Shao-Horn and co-workers have defined the ligand p band center that dictates E_H in a wide range of materials including metal oxides, phosphates, fluorides, and sulfides.[85] Generally, materials with higher ligand p band center energy (i.e., closer to the Fermi level) have a lower E_H. In addition, this correlation was applied to predict the activity (or stability) of organic electrolyte molecules (such as ethylene carbonate) on the oxide electrode surface in Li-ion batteries.[86] The energy of dissociated products decreases with the increasing of O 2p band center (Figure 4e), indicating a more favorable C–H bond dissociation of ethylene carbonate by high valent oxides with Fermi level approaching the oxide O 2p band. Similarly, O 2p band center has been proposed to correspond with the E_O on the surface of metal oxides and perovskite oxides.[74,87] Recently, Nørskov and co-workers have demonstrated a linear positive correlation between average O 2p state energy (a similar but more site-specific descriptor than O 2p band center) and E_O across different metal and metal-oxide surfaces.[88,89] Combining these findings with the E_{TS}–E_H correlation will allow for the rational design of methane activation catalysts based on their band structures and electronic properties.

The activity descriptors are established based on the methane-to-methanol conversion pathway assuming C–H bond activation as the rate-limiting step, whereas the side reactions of the reaction network (Figure S1, Supporting Information) are omitted. We assume that the energetics in C–H bond activation scale with the activation barriers for all elementary steps, which has been confirmed for the oxidation of hydrocarbons and oxygenates (including C1–C4 alkanes, alkenes, alkanols, and alkanals) on oxides.[10] Therefore, the descriptor for C–H bond activation of methane is still expected to describe the reaction kinetics of side reactions as well. But the correlation between overall reaction kinetics and activity descriptors can be influenced when side reactions are considered, which requires further studies.[58,59]

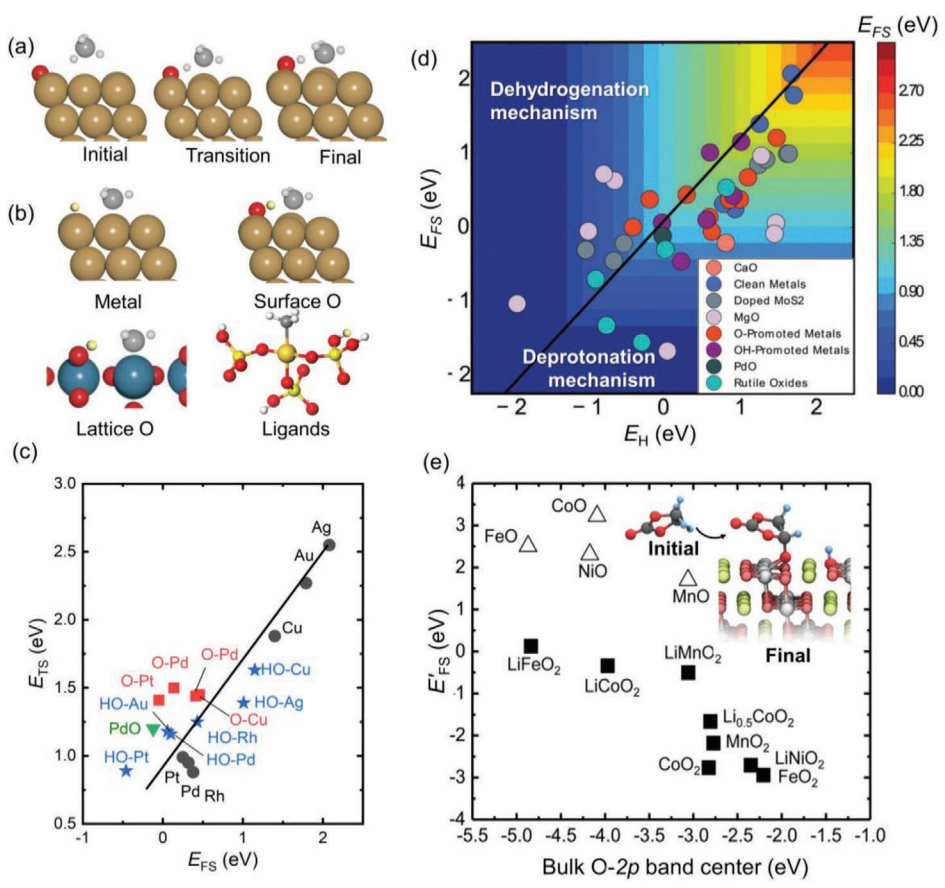

Figure 4. a) Structural representation of the initial state, transition state, and final states of the deprotonation mechanism. The activation process is essentially the deprotonation of CH_4 on the surface which can be written as $CH_4 \rightarrow CH_3^-$(metal) + H^+(acceptor). b) Examples of possible proton acceptors including surface metals (Pt), surface oxygens (O-Pt), lattice oxygen (IrO_2),[22] and ligands (Pd-H_2SO_4).[49] c) Universal scaling relationship between transition state energy (E_{TS}) and final state energy of CH_4 deprotonation on the surface (E_{FS}). d) E_{TS} as a function of E_{FS} and hydrogen affinity (E_H) as descriptors. The black line, defined by the equation of $E_{FS} = 1.12E_H + 0.07$, indicates two descriptors predicting equal E_{TS}. e) The final state energy of the dissociated configuration of ethylene carbonate on metal oxide surface (E'_{FS}) as a function of the O 2p band center. Inset shows the initial ethylene carbonate and dissociated products on metal oxide surface, which can be written as $(OCH_2CH_2O)CO + 2Mn^+ \rightarrow (OCHCH_2O)CO^+$(on metal) + H^+ (on oxygen) + $2M^{(n-1)+}$. Reproduced with permission.[22] Copyright 2017, Royal Society of Chemistry.

3.2. Selectivity Descriptor

Analyses of current methane-to-methanol conversion systems reveal that these catalysts fail to simultaneously maximize methane conversion and methanol selectivity.[13,21] The conversion/selectivity trade-off stems from the underlying thermodynamic limitations of the system wherein the C—H bond dissociation energy of methane is ≈40 kJ mol^{-1} higher than that of methanol. A scaling relationship between activation energy of methane and methanol (abstraction of the C—H hydrogen, **Figure 5**a) exists across a vast scope of catalysts operating via the dehydrogenation mechanism, including metals, metal oxides, metal-exchanged zeolites, metal-embedded graphene, and metal–organic complexes (Figure 5b).[90] The conversion/selectivity limit was modeled by Nørskov and co-workers using a simple two-step reaction model ($CH_4 + 0.5O_2 \rightarrow CH_3OH$; $CH_3OH + 1.5O_2 \rightarrow CO_2 + 2H_2O$),[90] where two steps are irreversible and their corresponding rate constants are denoted as k_1 and k_2. The selectivity toward methanol is given by Equation (2), where X is the conversion of methane and ΔG_a is the activation energy difference between methane and methanol

$$\text{Selectivity} = \frac{1-X-(1-X)^{k_2/k_1}}{X(k_2/k_1-1)} = \frac{1-X-(1-X)^{\frac{\Delta G_a}{k_B T}}}{X\left(\frac{\Delta G_a}{k_B T}-1\right)} \quad (2)$$

The conversion–selectivity limit for most catalysts falls within the prediction of Equation (2) (Figure 5c). This equation predicted ≈0.01% conversion to achieve 50% methanol selectivity at 423 K, indicating a low conversion or selectivity without methanol protection. Similar to the strategy of protecting reactive products during the biomass conversion,[91] Nørskov and co-workers proposed several strategies to overcome the limitation in methane conversion to methanol, including 1) employing methanol "collectors" or "protectors" to reduce methanol partial pressure (i.e., activity), 2) applying aqueous reaction conditions

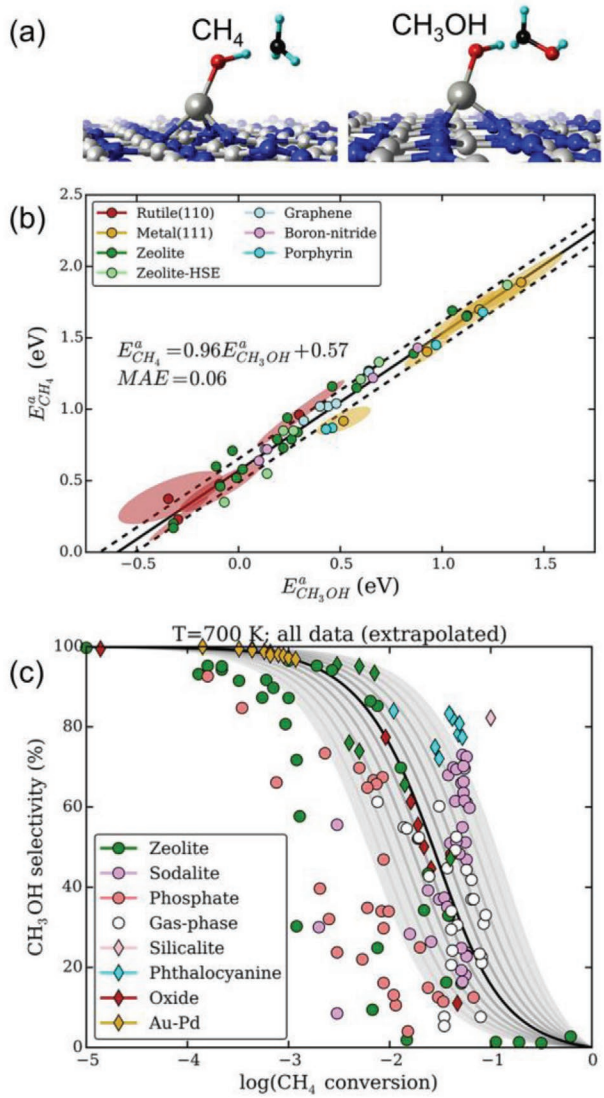

Figure 5. a) Structure of C–H bond cleavage transition states for CH_3OH and CH_4 on a representative catalytic center of oxygen-promoted Pd@BN. b) Activation energy scaling relationship for methane and methanol. The standard deviation of mean is indicated by dash lines. c) Comparison of experimental methane conversion and selectivity of methanol yield with the prediction of Equation (2). Experimental data were extrapolated to the gas phase at 700 K. Gray lines and shading indicate a ±1 σ error. Reproduced with permission.[90] Copyright 2018, American Chemical Society.

to stabilize methanol by solvation, and 3) using diffusion-limited catalysts that lower the ΔG_a to achieve high selectivity.[90] With the diffusion of both methane and methanol as the rate-limiting step, the difference between apparent activation energies will approach zero, leading to an increase in methanol selectivity at a certain conversion. The idea of designing diffusion-limited catalysts has been realized recently in a supramolecular catalyst that incorporates a hydrophobic hemicryptophane cavity around Cu, Fe, and V metal centers.[92] The methane-to-methanol selectivity of metal centers was shown to increase by confinement of the cavity. The methanol "collectors" idea is conceptually related to the widely adopted methanol protection schemes by stabilizing methane in the form of a methyl ester which can be hydrolyzed afterward to recover methanol.[42] The effect of aqueous solution on stabilizing methanol explains the generally higher conversion and selectivity delivered by liquid-phase reactions (e.g., aqueous H_2O_2 solutions) than gas-phase systems.[13] The selectivity descriptor not only explains the conversion–selectivity limitation of current catalysts, but also guided the design of diffusion-limited catalysts to achieve high selectivity beyond the limitation.

3.3. Toward Establishing Design Principles of Thermal Catalysts

We will review homogenous and heterogenous partial methane oxidation catalysts used both thermal and electrochemical conditions to rationalize their design principles. This review does not intend to cover the vast scope of homogenous and heterogenous catalysts; instead, we will use representative catalysts as examples to rationalize the activity/selectivity trends based on the aforementioned reaction mechanisms and descriptors. We will discuss their intrinsic limitations (e.g., regeneration of active sites) and provide suggested paths for the design of future electrocatalysts beyond the current state of art. We have divided the catalysts into two categories based on the reaction pathways (either dehydrogenation (radical) or deprotonation (surface-stabilized)) they typically follow.

3.3.1. Thermal Catalysts that Undergo Dehydrogenation Mechanism

Cu- and Fe-exchanged zeolites have been vastly studied as methane oxidation catalysts,[40,93] due to their structural similarity with Cu- and Fe-active centers in particulate methane monooxygenase (pMMO) and soluble methane monooxygenase (sMMO).[94] Actually, the reaction rate predicted by the G_f descriptor shows that Cu—O-based zeolites (Cu-O-Cu/MOR,[70] bis-μ-oxo-Cu/MOR,[19] and Cu_3O_3/MOR[71]) lie close to the top of the volcano plot. The slightly different E_{TS} of Cu-based zeolite series can be attributed to the structural diversity of metal centers. For example, the Cu–O–Cu angle (dictated by the zeolite structures) is believed to affect the orbital energy of $[Cu_2(\mu\text{-}O)]^{2+}$ sites and subsequently change the methane activation energy.[95]

The reaction mechanism of Cu—O-based zeolites involves 1) CH_4 activation by hydrogen abstraction to form •CH_3 and •OH radicals, 2) radical rebound to form methanol, and 3) methanol desorption and catalyst regeneration by oxidants (**Figure 6**a).[55] Conventionally, the catalytic conversion of methane to methanol by Cu-based catalysts uses N_2O or H_2O_2 as oxidants. To improve selectivity, a two-step methane oxidation scheme was developed where Cu-zeolites were activated by O_2 oxidation at a high temperature (450 °C), and subsequently reacted with methane at a milder temperature (200 °C) without O_2 to protect overoxidation of methanol.[19] Later on, the use of water as the oxidant to produce active Cu—O—Cu sites in zeolites was reported following a similar two-step scheme (activate catalyst at 400 °C followed by anaerobic oxidation of methane at 200 °C). However, this nonisothermal process requires a

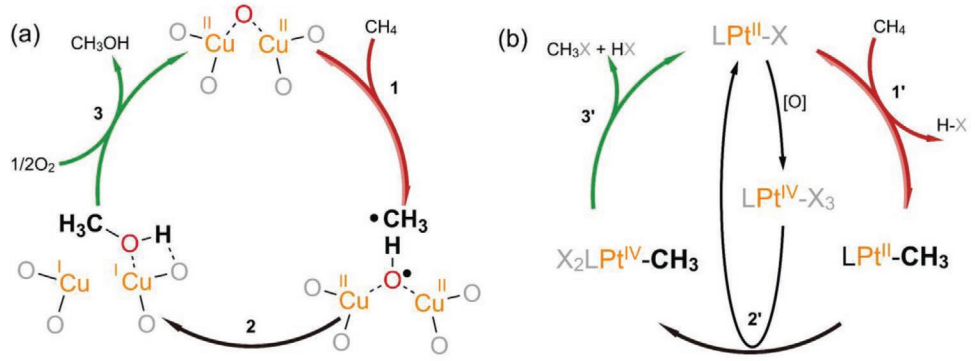

Figure 6. Schematic representation of methane partial oxidation to methanol on Cu-zeolites[55] and [(2,20-bipyrimidine)$PtCl_2$][42,83] with dehydrogenation and deprotonation mechanism, respectively. a) Cu-zeolite catalyzed methane oxidation involving 1) C—H activation and •CH_3 radical initiation, 2) radical rebound, and 3) methanol desorption and catalyst regeneration. b) The Periana system with Pt^{II} centers involving 1) C—H activation and Pt^{II}—CH_3 bond formation, 2) Pt^{II} oxidation, and 3) reductive elimination.

temperature swing of 200 °C to stoichiometrically produce methanol which hinders the practical applications.[96] Recently, Romań-Leshkov and co-workers have demonstrated the continuous catalytic methane partial oxidation at steady state by co-feeding O_2 and water with the aid of Cu-SSZ-13 at mild temperature (≈220 °C).[41] Follow-up mechanistic studies indicated that the active site was a $[Cu—O—Cu]^{2+}$ motif.[97] It was also observed that a high alumina content was necessary to prevent the overoxidation of methane to CO_2. Another recent mechanistic study using Cu-ZSM-5 zeolite clarified the reaction mechanism by electron paramagnetic resonance (EPR) and solid-state NMR.[55] The authors illustrated evidence that methane is activated at the $[Cu—O—Cu]^{2+}$ site to form •CH_3 and •OH radicals. This led to the conclusion that the generated methanol was stabilized by the closed Al—O moiety, which prevented the overoxidation of methanol. Although the Al content in zeolites should not affect the activity of Cu centers, it alters the geometry of the active center leading to a remarkable shift in the selectivity. Besides the nature of the active center, the zeolite framework also affects C–H activation by stabilizing certain $Cu^{2+}\cdots$alkane intermediates in the cavity via confinement effects. This was demonstrated by Giamello et al., who attributed the different C_3H_8 conversion levels observed in Cu-TNU-9 (80%) and Cu-Y (10%) at 350 °C to the selective formation of $Cu^{2+}\cdots C_3H_8$ intermediates in the cavity of Cu-TNU-9.[98] While the methane oxidation activity can be affected by the structure of Cu species and the cavity environment of Cu-containing zeolites, the G_f descriptor still provides a reasonable estimation of different types of Cu-zeolites.[99]

Iron is another attractive catalyst center for the partial oxidation of methane. However, Fe-based zeolites have brought less attention compared to Cu-based zeolites due to the limited formation of active sites by molecular oxygen. Conventionally, strong oxidants such as N_2O or H_2O_2 are used to activate Fe-zeolites.[15,16] A recent DFT study indicates that the mechanism of methane oxidation by Fe/ZSM-5 catalysts using H_2O_2 at room temperature is a combination of dehydrogenation, deprotonation, and Fenton pathways.[56] The reason for such complexity is caused by the presence of multiple oxidation states of Fe species. Fe^{II} and Fe^{III} have been shown to promote the deprotonation and Fenton pathways, whereas Fe^{IV}–O has been shown to catalyze the dehydrogenation pathway. The mechanistic study also showed that the geometry of the Fe cluster does not dramatically affect the catalyst's activity, but the structure of zeolites does alter the reaction steps. Similarly, Bao and co-workers have reported a graphene-confined Fe single atoms catalyst, which contains an FeN_4 active site.[54] Using H_2O_2 as the oxidant at room temperature, this catalyst converts methane into a series of C_1 liquid products including CH_3OH, CH_3OOH, $HOCH_2OOH$, and HCOOH. Recently, Tabor et al. have observed the formation of Fe^{IV}–O from O_2 at room temperature by a pair of distant Fe^{II} centers stabilized in the matrix of a zeolite. This delicately designed binuclear Fe^{II} site converts methane into methanol at room temperature using O_2 as oxidant, representing a breakthrough in methane oxidation catalysis.[100]

Recently, Weaver and co-workers were able to experimentally prove that IrO_2 is a highly active catalyst for methane oxidation as predicted by the G_f descriptor in the rate volcano plot (Figure 3c).[12] It was observed that methane underwent facile C—H bond cleavage and formed a strong σ bond on the IrO_2 (110) surface at a low temperature (–98 °C). Such a phenomenon suggested that the reaction occurs by a deprotonation mechanism at low temperature, rather than a dehydrogenation mechanism. These experimental results were inconsistent with the simulations done by Nørskov and co-workers that suggested a dehydrogenation mechanism.[69] The inconsistency can be explained by the differences in the surface oxygen coverage between the computational model and the experiment. The computations by Nørskov and co-workers considered an oxygen promoted surface where Ir coordinatively saturates with surface oxygen, leaving no open metal sites. While Weaver and co-workers used a stoichiometric amount of IrO_2 under ultra-high-vacuum conditions to react with methane, which contrary to Nørskov and co-workers' model, possesses free Ir sites to form Ir—CH_3.[12] Unfortunately, the high reactivity of the catalyst alone does not make it suitable for methane oxidation as the overoxidation is almost inevitable, resulting in CO and CO_2 as main products.

3.3.2. Thermal Catalysts that Undergo Deprotonation Mechanism

The deprotonation mechanism is commonly observed in homogenous catalytic reactions in polar mediums where metal exists in low oxidation states and proton acceptors are easily accessible. The activity descriptor E_{FS} was used to predict the activation barriers for catalysts with the deprotonation mechanism, which predicted noble metals Pd, Pt, and Rh as highly active catalysts (Figure 4c). Shilov et al.'s system is a classic example of these type of systems which enables the activation of methane through a deprotonation mechanism ($M-CH_3$ intermediates).[101,102] In an aqueous solution, $Pt^{II}Cl_2$ acts as catalytic centers and $[Pt^{IV}Cl_6]^{2-}$ acts as a stoichiometric oxidant allowing the conversion and stabilization of methane into CH_3Cl.[102] In line with this, Periana and co-workers designed an organic ligand-stabilized Pt^{II} complex, [(2,20-bipyrimidine)$PtCl_2$],[42] that converts methane into methyl bisulfate (CH_3OSO_3H) in concentrated H_2SO_4. This method achieved an ≈90% methane conversion and an 81% CH_3OSO_3H selectivity at 220 °C with a turnover frequency (TOF) of 36 h^{-1}. The concentrated H_2SO_4 acted as the solvent, methanol protector, and oxidant (SO_3). Both aforementioned protected methanol species, CH_3OSO_3H and CH_3Cl, could be hydrolyzed in a subsequent step to recover methanol. Mechanistic studies in these homogenous Pt-based catalyst systems revealed that the reaction proceeds through the following steps: 1) the C—H activation of the catalyst to form the $Pt^{II}-CH_3$ bond, 2) the Pt^{II} oxidation by SO_3 or other oxidants to form $Pt^{IV}-CH_3$, and 3) the reductive elimination to produce stabilized methanol and regenerate the Pt^{II} sites (Figure 6b).[49–51,83] The inactive $Pt^{IV}X_3$ species can be brought back by reacting with $Pt^{II}-CH_3$. This system was further optimized by Schüth and co-workers who achieved a significantly enhanced TOF of 23 000 h^{-1} with CH_3OSO_3H selectivity above 98% by using $K_2Pt^{II}Cl_4$ salts in oleum (20% SO_3/H_2SO_4) at 215 °C.[103] The SO_3 concentration was shown to change the activity by three orders of magnitude to realize the high TOF. Similar to Pt^{II} complexes, $Pd^{II}SO_4$ has also been used in the conversion of methane to CH_3OSO_3H in H_2SO_4, but at a lower temperature and TOF (160 °C and 0.6 h^{-1}, respectively).[104,105] $Pd^{II}SO_4$ could also be used to directly convert methane to acetic acid (selectivity of 90%) by an oxidative coupling in H_2SO_4 with a turnover number (TON) of 18 at 180 °C. This conversion of methane to acetic acid has been reported using other catalysts such as $RhCl_3$, which can achieve a selectivity of ≈95% in the presence of CO and O_2 at low temperatures, 95 °C.[103]

Unfortunately, regardless of the high activity, the practical application of Periana's system is limited by the expensive oxidant (SO_3), the high energy penalty to recycle protectors, and more importantly, the sensitivity toward water (the byproduct).[9] Detailed experimental and DFT calculations on the Periana's system indicates that the C—H activation step is even faster than the oxidation of Pt^{II} to Pt^{IV}, rendering the Pt^{IV} regeneration process the rate-limiting step.[83] However, the C—H activation rate is significantly suppressed by the generated water during methane oxidation, which then becomes the rate-limiting step at H_2SO_4 concentration below 60%. This is also accompanied by a drop of TOF from 10^{-3} to $<10^{-5}$ s^{-1}. In this regard, electrocatalysis could address the limitation of Periana's systems by regenerating high valent Pt^{IV} sites without the need of SO_3.

Although the deprotonation mechanism is mostly seen in homogenous systems, this mechanism has also been studied using heterogenous catalysts. The Periana's catalyst was recently heterogenized for methane activation by coordinating Pt^{2+} with the bipyridyl sites in a triazine-based covalent organic framework (COFs). This new catalyst leads to a 75% CH_3OSO_3H selectivity, which is comparable to the results from the homogenous systems.[106] Another study in methane oxidation was carried out over Pd/Al_2O_3 catalyst. However, the stability of the catalyst at high temperature was a big concern and it lost the activity presumably due to the Pd to PdO transition.[107] In line with this, a DFT study from Janik and co-workers suggested that methane oxidation on Pd/ceria surface is much faster compared to other Pd and PdO surfaces.[108] Typically, methane oxidation reaction catalyzed by noble metals requires high temperatures, which not only leads to the oxidation of the catalysts but also causes the complete oxidation (combustion) of methane to CO_2. Thus, noble metals by themselves are not considered suitable for methane oxidation in thermal catalysis. This drawback could be overcome by the redesign of the catalyst, specifically, by modifying the composition and/or morphology of the catalysts. For example, the single atom of Rh stabilized on ZrO_2 can catalyze the partial oxidation of methane into methanol using H_2O_2 as an oxidant, whereas Rh nanoparticles only produce CO_2 under the same conditions.[81] In situ diffuse reflectance infrared Fourier transform spectroscopy and DFT calculation showed that only the coordinatively unsaturated single Rh sites were able to stabilize $Rh-CH_3$ intermediates during the reaction. Another example of catalyst design to improve methanol selectivity was done by Hutchings and co-workers. They developed an alloy of Au-Pd nanoparticles supported on TiO_2, which reached a maximum selectivity of 49% using H_2O_2 at mild temperature (50 °C).[109] Later on, they significantly improved their catalyst design by synthesizing Au-Pd/TiO_2 colloids, which allowed the methane oxidation by molecular oxygen instead of H_2O_2.[110] Interestingly, in situ EPR experiments revealed the formation of radical intermediates, suggesting a mixed reaction mechanism that involves radical and surface stabilized pathways.

A major limitation for many state-of-art catalysts (operating via either the dehydrogenation or the deprotonation mechanism) is the (re)generation of active sites rather than the C–H bond activation. This corresponds to the weak oxygen-binding materials in the rate volcano plot, in which low active site coverage limits the reaction rate (Figure 3c). For example, activation of Cu- and Fe-zeolites by O_2 usually requires a higher temperature than the C–H bond activation. Similarly, the Pt^{IV} regeneration step is shown to be slower than the C—H activation step in Periana's system. Enhancing reaction rate (i.e., active site formation rate) in thermal catalytic systems can be achieved at elevated temperatures, but this inevitably leads to the uncontrolled overoxidation of methanol to CO_2 as the thermodynamic sink. Strong oxidants such as H_2O_2 can be used to regenerate active sites at a lower temperature, but extra cost also adds to the whole process. Electrochemistry provides a possible solution to address the limitation of current thermal catalysts: the active sites can be easily regenerated by applying potentials to avoid high temperatures and/or expensive oxidants.

3.4. Toward Establishing Design Principles of Electrocatalysts

There is no intrinsic distinction in the C—H activation step of methane partial oxidation between thermal and electrocatalysts. Both thermal catalytic and electrocatalytic methane oxidation proceed through the formation of oxygenated active sites and the subsequent oxidation of methane.[3] The active sites are (re)generated by chemical oxidation ($M + 0.5O_2 \rightarrow M{-}O$) or electrochemical oxidation ($M + O^{2-} - 2e^- \rightarrow M{-}O$) in thermal catalysis and electrocatalysis, respectively. While electrochemistry generates oxidative catalytic sites by controlling electrode potentials, methane activation is essentially a thermochemical step. Consequently, some electrocatalysts bear similar metal centers as thermal catalysts, such as Pd, Pt, V, Ru, and Ir.[24] Based on the understanding of thermal catalysts, it is expected that methane activation on Pd- and Pt-based electrocatalysts would undergo the deprotonation mechanism, whereas metal oxide-based electrocatalysts would follow the dehydrogenation mechanism. However, the surface energy and oxygen coverage of electrocatalysts are constantly changing with the different applied potential. Thus, the reaction mechanism may differ depending on the catalyst as well as the operational conditions. In this section, we assign metal oxide electrocatalysts to the dehydrogenation mechanism and Pd/Pt-based electrocatalysts to the deprotonation mechanism.

3.4.1. Electrocatalysts that Undergo Dehydrogenation Mechanism

V_2O_5 is a widely used catalyst in the thermal catalytic oxidation of methane and it is found to be one of the most active non-noble metal electrocatalysts for methane selective oxidation.[33] The activity descriptor G_f predicts that the reaction rate of V_2O_5 is limited by the regeneration of high-valent active sites. Consequently, thermal catalytic methane oxidation by V_2O_5 catalysts usually requires high temperatures (>450 °C) and the use of strong oxidations such as N_2O.[43,44] Using the electrochemical method, the V_2O_5 catalyst can operate at milder conditions. In the discovery of nonplatinum-metal-based electrocatalysts, Lee and Hibino defined V_2O_5/SnO_2 as the optimal material for selective methane partial oxidation to methanol after screened a series of metal species (Mn_2O_3, V_2O_5, Fe_2O_3, Au, Co, Pd, Pd Ru, MoO_3, Ag, and CrO) supported on different matrices (SnO_2, WO_3, MoO_3, ZrO_2, Fe_2O_3, CeO_2, and TiO_2).[33] Based on this finding, a fuel cell type reactor was built where methane and water vapor were co-fed to the V_2O_5/SnO_2 anode while the air was supplied to the corresponding cathode. By judicious tuning of the reaction temperature, the V_2O_5 content, and the anode potential, the system reached a current efficiency and methanol selectivity of 61.4% and 88.4%, respectively, at 100 °C. Given the high oxidation state of V^{5+} and its weak interaction with $-CH_3$, this catalyst is expected to drive the methane oxidation to methanol through a dehydrogenation mechanism. When compared to the thermal catalytic V_2O_5-based process, this electrochemical approach led to increased reaction rate and selectivity (the maximum yield appeared at a cell potential of 0.8 V and no product was observed without applying potential) without the need of nonrecyclable/toxic external oxidants such as N_2O or SO_3 (usually used for the regeneration of V_2O_5 catalysts).[43,44] Very recently, vanadium (V)-oxo dimer clusters in H_2SO_4 (V_2-oxo/H_2SO_4) was used as electrocatalysts to convert methane into CH_3OSO_3H at room temperature.[109] A high turnover frequency of 1336 h^{-1} was achieved under 3 bar methane, which is significantly higher than that obtained under thermal catalytic conditions (≈2 h^{-1}, 40 bar methane). This electrochemical methane oxidation system showed stable performance for 240 h and a 90% Faradaic efficiency.

RuO_2, with similar G_f as that of IrO_2 in the rate volcano plot (Figure 3c), has also been used to build a $TiO_2/RuO_2/V_2O_5$ gas diffusion electrode in 0.1 mol L^{-1} of Na_2SO_4 electrolyte.[111] A current efficiency of ≈30% for methanol formation was observed at 2.0 V (vs saturated calomel electrode) along with the formation of 40% formic acid, 10% formaldehyde, and 20% oxygen. The addition of 5.6% V_2O_5 to the TiO_2/RuO_2 electrode was shown to double the methanol formation rate and selectivity while suppressing the formation of formic acid and formaldehyde.

An active electrocatalyst does not necessarily have to belong to the subset of materials active in thermal processes. Metal oxides, such as NiO and Co_2O_3, are inactive thermal catalysts but are active for electrocatalytic methane oxidation.[112–114] This phenomenon could be explained by the changes in the metal oxidation states and surface free energies by electrode potential, resulting in a nonequilibrium population of a highly reactive M—O sites. The high-energy M—O sites are difficult to form thermochemically using O_2 (i.e., high G_f), but they can be generated by applying an anodic potential.[29] $Ni(OH)_2$,[112] NiO/ZrO_2,[113,114] and Co_2O_3/ZrO_2[115] have been explored as anode catalysts for methane activation at room temperature in carbonate electrolyte. The generation of methanol and higher alcohols such as propanol was observed by ^1H NMR or MS, but the TOF, TON, and Faradic efficiency were not qualified possibly due to the low yield.

3.4.2. Electrocatalysts that Undergo Deprotonation Mechanism

A representative example that bridges thermal catalysis and electrocatalysis has been demonstrated by Surendranath and co-workers where they reported the rapid and selective electrochemical oxidation of methane into CH_3OSO_3H and methanesulfonic acid (CH_3SO_3H) using a $Pd^{II}SO_4$ catalyst in oleum (20% SO_3/H_2SO_4).[30] This electrochemical methane oxidation system is inspired by the thermal catalytic Periana system which uses Pt^{II}-based catalysts and concentrated H_2SO_4 as the solvent, oxidant, and methanol protector. In the electrocatalytic system, H_2SO_4 plays an additional role as the electrolyte. Under anodic potential, the electrochemical methane oxidation system achieves a high reaction rate (TOF of 2300 h^{-1}) and good selectivity (≈93% for methane precursors CH_3OSO_3H and CH_3SO_3H) at 140 °C. This is ≈50 times higher than that of the Periana's catalyst (**Table 2**) and ≈10 times higher than the state-of-art Pt^{II}-based thermal catalyst under similar temperature and pressure.[116] The dramatically enhanced activity by electrochemical methods is attributed to the electrogenerated high-valent Pd^{III}_2 species that rapidly activate methane. The Pd^{III}_2 active sites catalyzed the Faradic and non-Faradaic reaction pathways to form CH_3OSO_3H and CH_3SO_3H (molar ratio 1:14),

Table 2. A list of representative catalysts for methane oxidation discussed in the review, their operational conditions, and catalytic performance.

Condition	Catalysts	T [°C]	P_{CH4} [bar]	Oxidant	TOF [mol_{CH3OH} mol_{cat}^{-1} h^{-1}]	Mechanism	Ref.
Heterogenous thermal catalysis	V_2O_5	80	51	H_2O_2	2.3[a)]	Dehydrogenation	[12]
	V_2O_5	180	40	SO_3	1.9	Dehydrogenation	[43]
	Cu-SSZ-13	210	1	O_2	0.0061	Dehydrogenation	[97]
	Cu-ZSM-5	210	1	O_2	0.0022	Dehydrogenation	[97]
	Cu-MOR	200	6	O_2	70.1[b)]	Dehydrogenation	[99]
	Cu-ZSM-5	200	6	O_2	23.9[b)]	Dehydrogenation	[99]
	Fe-ZSM-5	50	3[c)]	H_2O_2	2278	Dehydrogenation	[99]
	Cu-ZSM-5	50	3	H_2O_2	2113	Dehydrogenation	[99]
	FeN_4-C	25	18	H_2O_2	0.47[a)]	Dehydrogenation	[54]
	Pd/Al_2O_3	270–470	1	O_2	40[d)]	Deprotonation	[122]
	$AuPd/TiO_2$	50–90	30.5	H_2O_2	0.5–25.7[e)]	Mixed mechanisms	[109]
	$AuPd/TiO_2$	50	30	O_2, H_2O_2	1.5–4.8	Mixed mechanisms	[110]
Homogenous thermal catalysis	$PdSO_4$	160	69	SO_3	0.6	Deprotonation	[105]
	(bpym)$PtCl_2$	220	34	SO_3	36	Deprotonation	[42]
Heterogenous electrocatalysis	1%V_2O_5/SnO_2	100	0.1	O_2	—[f)]	Dehydrogenation	[33]
	$TiO_2/RuO_2/V_2O_5$	25	1	H_2O	—	Dehydrogenation	[111]
	$Ni(OH)_2$/MWCNTs	25	0–1	O_2	—	Dehydrogenation	[112]
	NiO/ZrO_2	25	0–1	O_2	—	Dehydrogenation	[114]
	Co_3O_4/ZrO_2	25	1	H_2O	—	Dehydrogenation	[115]
	Pt	80	2	O_2	—	Deprotonation[g)]	[123]
	Pt	660–800	0.3–0.5	O_2	—	Deprotonation[g)]	[34]
	Pd_8Au_1/C	50–250	0.5	O_2	—	Deprotonation[g)]	[32]
Homogenous electrocatalysis	V_2-oxo/H_2SO_4	25	3	O_2	1336	Dehydrogenation	[124]
	$PdSO_4$	140	7	SO_3	2300	Deprotonation	[30]
	$PtCl_2$	130	35	(VO)(SO_4)	0.34	Deprotonation	[118]

[a)]TOF based on total C_1 liquid products; [b)]TOF based on methane oxidation step (0.5 h) of activated Cu-zeolites. A full catalytic cycle consists of activation (8 h), methane oxidation (0.5 h), and methanol extraction with steam; [c)]30 bar 10% methane; [d)]TOF based on major products CO and CO_2; [e)]TOF based on the major product formic acid; [f)]Methane was overoxidized to CO and CO_2, or TOF of methanol is not reported; [g)]We assume Pd- and Pt-based electrocatalysts undergo deprotonation mechanism although the reaction mechanism may differ depending on operational conditions.

respectively. In other words, electrochemistry allows the sustainable formation of a nonequilibrium population of high-valent active metal sites by anodic polarization, whereas this process is usually sluggish in thermal catalytic systems. Moreover, Shilov et al.'s systems (Pt^{II} as a catalyst and Pd^{IV} as a stoichiometric oxidant) have been studied in electrochemistry[101,102] to turn the stoichiometric method into a catalytical process.[117,118] The expensive Pt^{IV} oxidant was regenerated electrochemically, leading to a continuous methanol production (TOF of 0.34 h^{-1}) with a comparable selectivity (70%) as stoichiometric methods.[118] For comparison, the chemical regeneration of Pt^{IV} either has a sluggish reaction rate or quickly depletes the catalytic Pt^{II} without good control. By combining the knowledge of electrochemical and thermal catalytic systems, these studies highlighted the capability of electrochemistry to overcome the thermodynamic limitations of thermal catalysis.

Pd and Pt electrodes have been extensively studied as the anode for methane oxidation in the exploration of hydrocarbons oxidation in fuel cells since the 1960s. Unfortunately, CO_2 has always been obtained as the major product at low temperature (<150 °C).[26] At elevated temperatures, methane to syngas (CO/H_2 = 1/2) is the dominant reaction pathway.[34,35] The high-temperature electrolysis is usually conducted in solid oxide fuel cell (SOFC) type reactors, in which Pt is used as an anode catalyst to activate methane (**Figure 7**a). The molecular oxygen is reduced at the cathode and O^{2-} is transferred through solid oxide electrolyte to the anode to fulfill the catalytic cycle. For example, Sobyanin and co-workers reported a methane to syngas conversion over a Pt-based anode in an SOFC reactor. This achieved a CO selectivity of 95% with a reaction rate of 3.6 mmol h^{-1} cm^{-2} at 800 °C.[34]

The valorization of methane oxidation into valuable products such as methanol and formaldehyde was demonstrated in the 1990s by Frese using Au and Cu as the cathodes with alkaline electrolytes at room temperature.[119] The formation of peroxide, and/or superoxide anions, has been proposed to initiate the methane activation by a radical chain reaction. A

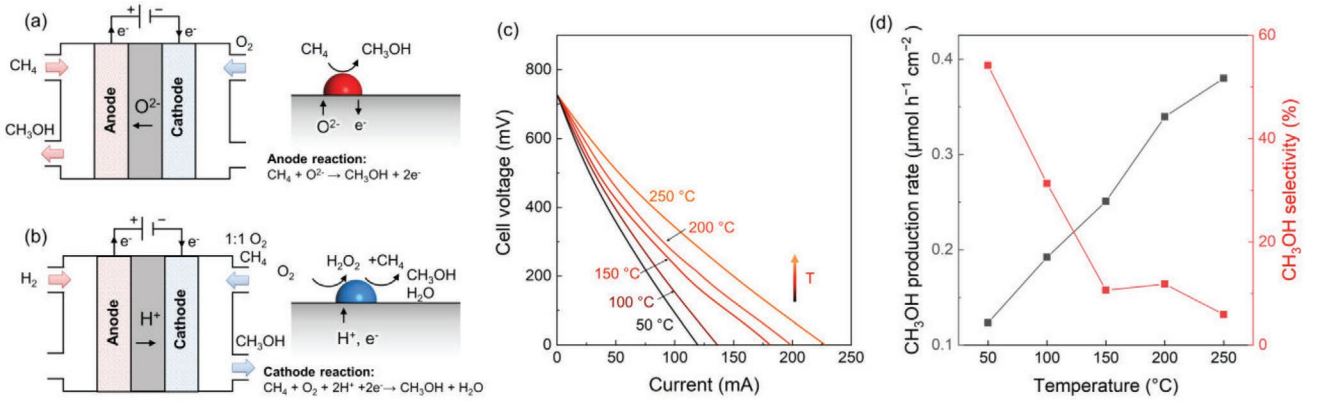

Figure 7. Schematic representation of a) a solid oxide fuel cell (SOFC) reactor with anodic methane oxidation[35] and b) a solid acid fuel cell reactor with cathodic methane oxidation.[32] c) Cell voltage–current curves of the fuel cell H_2, Pt/C | $Sn_{0.9}In_{0.1}P_2O_7$ (1 mm) | PdAu/C, 50% O_2 + 50% CH_4 at variable temperature. d) Methanol production rate and selectivity as a function of temperature. Selectivity defined by $n_{CH3OH}/(n_{CH3OH} + n_{CO2})$.[32]

similar concept was adopted to design a fuel cell with Pt/C as H_2 oxidation anode, Pd-Au/C as oxygen reduction cathode, and In^{3+}-doped SnP_2O_7 ($Sn_{0.9}In_{0.1}P_2O_7$) as proton conducting electrolyte (Figure 7b).[32] Methane was co-fed with oxygen to the cathode in a 1:1 ratio. The cell voltage–current density curves, at different temperatures, showed a constant open circuit potential of 740 mV and a temperature-dependent current (Figure 7c), possibly due to the reduced polarization resistance of the cathode and enhanced proton conductivity of the $Sn_{0.9}In_{0.1}P_2O_7$ electrolyte. The methanol production rate increased with temperature, whereas the selectivity decreased due to overoxidation (Figure 7d). Tuning the reaction temperature and current led to an optimized methanol production rate of 0.38 μmol h^{-1} cm^{-2} at an applied current of 400 mA cm^{-2} at 250 °C with a methanol selectivity of ≈6% (CO_2 as the main product). The Faradic efficiency for methanol production was lower than 0.01% because the predominant cathode reaction is oxygen reduction to water instead of methane-to-methanol conversion. The methane activation in this fuel cell reactor is likely to be a two-step process involving the generation of H_2O_2 and subsequent reaction with methane. The reaction pathway is similar to the previously reported Pd—Au nanoparticles catalyst, which showed a methane-to-methanol selectivity of 92% in aqueous H_2O_2 at 50 °C.[110] This catalytic performance is possible due to the production of hydrogen peroxide from the reduction of oxygen by the Pd–Au alloys that can further oxidize methane to methanol.[120,121]

These two types of fuel cell design, shown in Figure 7a,b, lead to intrinsically different reaction mechanisms. For fuel cells with a methane oxidation anodes (Figure 7a), the electrochemical process produces high-valent active metal sites or surface oxygen that subsequently catalyze the C—H activation via the deprotonation or the dehydrogenation mechanisms. The activity of these catalysts can be estimated by the G_f or the E_{FS} as descriptors. However, in the fuel reactors that oxidize methane on cathodes (Figure 7b), the C–H activation is usually initiated by the oxygen reduction products (H_2O_2 or •OH radicals). We have summarized the representative thermal and electrocatalysts for methane oxidation in Table 2 including their compositions, operational conditions, catalytic performances, and possible reaction mechanisms.

4. Potential and Perspectives of Electrocatalysis

4.1. Opportunities for Electrocatalytic Systems

The advantages of electrochemistry can be summarized by addressing the limitations of thermal catalysts in the partial oxidation of methane. The following aspects are considered the most crucial: 1) reaction rate, 2) methanol selectivity, and 3) process operational cost.

4.1.1. Reaction Rate Enhancement

It is well known that the reaction rate of charge transfer reactions can be controlled by the potential of electrochemical cells.[28] The applied potential on the electrode directly dictates the surface free energy and modifies the thermodynamic landscape of reaction,[28] which represents a higher degree of tuning compared to the control of temperature and pressure in thermal catalysis. Furthermore, the applied potential at the electrode surface modifies the adsorption energy of the reaction intermediate and regulates the reaction kinetics. In the case of methane activation through dehydrogenation mechanism, the formation of active M—O sites can be promoted by varying the electrode potential, which leads to a nonequilibrium population of active sites. The manipulation of applied potential can significantly accelerate the methane activation kinetics, especially for weak oxygen-binding materials (high G_f), in which the generation of M—O active sites is the limitation of methane activation. For methane oxidation catalysts that undergo through the dehydrogenation pathway, the electrochemical process can facilitate the formation of oxygen species (known as promoters or H^+ acceptors) on the metal surface.

This has been demonstrated to reduce the E_{TS} energy and promote the methane activation on Au and Ag surface, which is limited by the low oxygen coverages under conventional thermal conditions.

4.1.2. Improvements in Methanol Selectivity

Although overoxidation is thermodynamically inevitable, electrocatalysis offers precise control over the reaction kinetics to impart methanol selectivity. A constant difference of ≈40 kJ mol^{-1} between the activation energy of methane and methanol exists across a wide range of catalysts,[90] which is not likely to be changed by electrochemistry. However, it has been proposed that the methanol selectivity can be increased by controlling diffusion kinetics. For example, in the study of V_2O_5/SnO_2 anodic methane partial oxidation to methanol in a fuel cell type reactor, the reaction rate and methanol selectivity were finely tuned by cell potential and reaction temperature, achieving 88.4% methanol selectivity and ≈~0.3% conversion at 100 °C. Both, reaction rate and selectivity, were higher than the thermal V_2O_5/SiO_2 catalytic system using O_2 as an oxidant.[44] Nonetheless, a systematic study to reveal the effects of potential, current, temperature, pressure, and electrolyte on the selectivity is required.

In addition to the kinetic control, methanol can be stabilized by solvation or chemical transformation to increase its selectivity at high conversion. Aqueous electrolytes used in most electrocatalysis are expected to stabilize methanol due to the more favorable solvation free energy of methanol than methane.[90] Methanol protectors such as H_2SO_4 could convert methanol into more stable methyl esters to avoid overoxidation.[42] These protectors are also widely used electrolytes and therefore can be easily adopted in electrocatalysis. However, protection strategies usually introduce extra steps to regenerate methanol from its methyl esters, adding an energy penalty to the process. A techno-economic analysis is necessary to evaluate the cost added by protection/deprotection steps.[37]

4.1.3. Decreases in the Operational Cost

Electrochemical methods enable the activation of methane at low temperatures by the electrochemical generation of active M–O sites without the necessity of expensive oxidant such as N_2O, H_2O_2, SO_3. Such methods could potentially reduce the operational cost of thermal catalytic systems that require either high thermal energy or strong oxidants. For example, H_2O_2, a widely used oxidant, allows selective methane activation at near room temperature over a variety of catalysts such as Pd–Au[32] and FeN_4–C[54] as discussed previously. However, H_2O_2 (0.67 \$ kg^{-1}) is even more expensive than methanol (0.35 \$ kg^{-1}), making this H_2O_2 promoted methanol synthesis unprofitable.[125] A previous work demonstrated that H_2O_2 can be generated in situ by the electrochemical reduction of oxygen and react with methane at a Pd–Au cathode.[120,121] Other expensive stoichiometric oxidants such as Pt^{IV} can also be regenerated electrochemically, as discussed in the electrocatalytic Shilov and Periana's chemistry.[117,118] More importantly, the electrochemical schemes are modular, as the productivity scales directly with electrode size and current density. Therefore, the electrochemical methane-to-methanol device can serve as a modular and cost-effective solution for both large-scale industrial plants and in smaller quantities. The small-scale electrochemical methane-to-methanol device is especially pragmatic in remotely located oil fields where centralized methane-steam reforming infrastructures are not available.[126] A techno-economic analysis will be helpful to evaluate the electronic process by taking into consideration of the capital cost, electricity, and methanol separation.[37] Additionally, life cycle assessments can be applied to quantitatively compare the electrocatalytic methane-to-methanol techniques to current strategies (i.e., steam reforming and methanol synthesis) and other possible routes (e.g., methanol synthesis from syngas and electrolytic hydrogen).

4.2. Perspectives in the Electrocatalytic Conversion of Methane to Methanol

We surmise that the future development of electrocatalysts will be centered on the design of electronic structures of metal centers under the guidance of mechanistic understandings and activity descriptors. Based on the activity descriptor, an exploration of weak oxygen-binding materials such as SnO_2 and TiO_2[29] may lead to more active electrocatalysts that form highly reactive M–O active sites under an anodic potential. The anodic potential applied to the electrode will not only favor the formation of high-valent metal sites that are difficult to generate thermally, but also avoid the use of expensive oxidants. Stemming from these concepts, many more materials can be explored as potential electrocatalysts to address their thermal catalytic limitations. For example, single Fe stabilized on graphene is known to activate methane with H_2O_2 to generate Fe^{IV} active sites.[54] This Fe^{IV} active site may be generated electrochemically, thus, avoiding the use of external H_2O_2 oxidant. The steady Fe^{IV} sites can also prevent unwanted competing reactions at the Fe^{III} sites via an uncontrolled Fenton pathway. Similarly, single Pt^{II} stabilized on COFs,[106] as an immobilized Periana's catalyst,[123] may work electrocatalytically without the use of SO_3 oxidants.

Beyond electronic tuning, the activity and selectivity of electrocatalyst can be potentially optimized by noncovalent interactions. Changing electrolytes with different ions is expected to affect the solvent structure and oxidation reaction kinetics at the electrode/electrolyte interface.[127] The surface modification of electrodes with proton donor/acceptor layers with variable pK_a may affect the proton transfer and, in turn, accelerates the dehydrogenation/deprotonation of methane. Designing diffusion-limited electrocatalysts using porous materials with intrinsic cavities such as porous organic cages, MOFs, and COFs, seems to be a promising method to increase the selectivity. This has been exemplified by the supramolecular catalyst with confined hemicryptophane cages for methane oxidation showing enhanced selectivity than nonconfined catalysts.[92] Furthermore, the active site environment within the confined cavity can be judiciously designed for independent tuning of the binding energy of methane and methanol in order to break the conversion–selectivity limit of conventional catalysts. In addition, analyses of reaction networks for methane oxidation

(Figure S1, Supporting Information) can provide fundamental insights into the reaction mechanisms and guide the catalyst design efforts.[58,59] By understanding the possible reaction pathways, and avoiding unwanted pathways, the catalytic activity and selectivity can be optimized.

Despite the aforementioned merits of electrocatalysis in methane activation, these systems also encounter several challenges including high overpotential, competing reactions of unstable solvents/electrolytes, electrode restructuring under applied potential, and difficulty in methanol recovery. The fundamental limitations of electrocatalytic methane oxidation have been predicted by Rossmeisl and co-workers.[29] Based on DFT calculations, less oxophilic materials (high E_O) tend to form more reactive M–O sites, which leads to a lower methane activation barrier. But the active M–O sites require a higher potential to be (re)generated, and essentially lower the Faradic efficiency because of competing OER and uncontrolled overoxidation. Considering this, an ideal catalyst should have a weak oxygen-binding but still allow the OER under the applied potential. The chemical stability of electrolytes needs to be studied under methane oxidation conditions as well. Electrolytes that are stable toward the oxidation of active sites, such as H_2SO_4, are preferred.[30,124] In addition, the well-documented chemical dynamics of electrodes may lead to complex transformations of catalysts under applied potentials,[128] which requires further studies during electrochemical methane oxidation. The recovery of methanol from aqueous electrolytes is also difficult, which may demand an energy-intensive distillation process or membrane separation. It is even more challenging considering the low methanol concentration (< 1%) obtained in electrolytes to avoid overoxidation. In this regard, solid-state fuel cell reactors may be advantageous for methanol separation.

Besides electrocatalysts, some additional issues need to be considered for practical applications on the device level. For example, high-pressure methane is usually required in thermal catalysis to increase the surface methane coverage for gas-phase reactions at high temperature (>100 °C) or enhance the methane solubility for liquid-phase reactions at low temperature (<100 °C). However, current methane oxidation fuel cells usually operate at ambient pressure. This problem has been addressed by designing high-pressure fuel cell reactors that can operate at a pressure up to 40 bar,[129] or using gas-diffusion electrodes with high surface areas to enhance methane transport and reaction at a gas–liquid–-solid interface.[111] The deactivation of catalysts by sintering or coking in thermal catalysis at high temperatures hinders the long-term stability of catalytic systems under practical conditions. In this regard, the electrochemical methane conversion process operating at low temperature has been shown to enhance catalyst stability by reducing coke formation and sintering.[34,35] Furthermore, the development of proton or oxygen ion conductors with high ion conductivity at intermediate temperatures is required to make the electrochemical methane-to-methanol scheme practical.[37]

In terms of catalytic tests, many experiments have observed the generation of methanol without knowing the carbon resources. The electrochemical cell and fuel cell may be contaminated by alcohols during the electrode preparation or membrane assembly. Isotope labeling experiments using ^{13}C-labeled methane will confirm methane as the carbon resource. Unfortunately, the quantification of the catalytic efficiency (e.g., TOF and turnover number) is not commonly reported in the study of electrocatalysis hindering the direct comparison of catalytic performance with the benchmark thermal catalysts. Additionally, the distribution of methane oxidation products under different reaction conditions need to be determined to reveal the role of potential, current, temperature, pressure, and electrolyte on the catalytic performance. Furthermore, the characterization of reaction intermediates by in situ and ex situ surface sensitive techniques (such as IR, Raman, X-ray absorption spectroscopy, and X-ray diffraction techniques) is necessary to understand the reaction mechanism and guide the improvement of future catalysts.

5. Conclusions

The direct methane-to-methanol conversion has been considered as one of the "holy grail" reactions in the field of catalysis. Immense efforts have been made over the past decades, especially in the field of thermal catalysis, without yielding any catalysts that attract industrial attention. A brief review of current catalytic systems reveals that most thermal catalysts either require O_2 oxidant at a high temperature (> 200 °C) or strong external oxidants (H_2O_2, N_2O, and SO_3) at a lower temperature (< 200 °C) to generate active sites and activate inert C—H bonds. Overoxidation is almost inevitable under harsh conditions without methanol protection. Electrochemistry has been proposed as an alternative to address the inherent limitation of thermal catalytic systems. Specifically, the electrochemical method generates high-valent metal sites for C–H bond activation without the necessity of strong oxidants or high temperatures, while allowing precise control of reaction kinetics to maximize the selectivity. We classified methane activation catalysis into two basic mechanisms—dehydrogenation and deprotonation, which helps provide a fundamental understanding of methane activation and guide the rational design of electrocatalysts. Based on two reaction mechanisms, activity descriptors have been evaluated using hydrogen affinity E_H, M–O active site formation energy G_f and final state energy E_{FS}. More fundamentally, these descriptors have been correlated to the intrinsic electronic structures and properties such as the O 2p band center. Under the guidance of reaction mechanisms and activity descriptors, promising electrocatalyst candidates have been discussed and possible methods to enhance the activity and selectivity by electrochemistry have been proposed. Grand challenges remain in the development of direct methane-to-methanol conversion process. The activity and selectivity descriptors only provide an initial direction in the catalyst screening. More detailed experimental data and mechanistic studies are needed in future research to identify suitable catalysts and refine the descriptors for a more precise prediction of catalytic performance.[46,53] We believe that vast opportunities exist by bringing the understandings of thermal catalytic methane oxidation into the electrochemical fields. The development of electrochemistry could significantly advance the mechanistic understanding of reaction kinetics and catalyst discovery, leading to efficient gas-to-liquid technologies.

Supporting Information

Supporting Information is available from the Wiley Online Library or from the author.

Acknowledgements

This work was supported by the MIT Energy Initiative (MITEI) Energy Research Seed Fund Program and the Toyota Research Institute through the Accelerated Materials Design and Discovery program.

Conflict of Interest

The authors declare no conflict of interest.

Keywords

C–H activation, electrocatalysts, heterogenous catalysts, homogenous catalysts, methane to methanol

Received: July 1, 2020
Revised: August 14, 2020
Published online:

[1] P. G. Levi, J. M. Cullen, *Environ. Sci. Technol.* **2018**, *52*, 1725.
[2] R. A. Kerr, *Science* **2010**, *328*, 1624.
[3] J. Clayden, N. Greeves, S. Warren, P. Wothers, *Organic Chemistry*, Oxford University Press, Oxford **2001**.
[4] P. Tang, Q. Zhu, Z. Wu, D. Ma, *Energy Environ. Sci.* **2014**, *7*, 2580.
[5] N. Muradov, in *Compendium of Hydrogen Energy*, (Eds: V. Subramani, A. Basile, T. N. Veziroğlu), Woodhead Publishing, Oxford **2015**, p. 489.
[6] C. Elvidge, M. Zhizhin, K. Baugh, F.-C. Hsu, T. Ghosh, *Energies* **2016**, *9*, 14.
[7] E. McFarland, *Science* **2012**, *338*, 340.
[8] R. Horn, R. Schlögl, *Catal. Lett.* **2015**, *145*, 23.
[9] N. J. Gunsalus, A. Koppaka, S. H. Park, S. M. Bischof, B. G. Hashiguchi, R. A. Periana, *Chem. Rev.* **2017**, *117*, 8521.
[10] P. Deshlahra, E. Iglesia, *J. Phys. Chem. C* **2016**, *120*, 16741.
[11] Z. Liu, D. C. Grinter, P. G. Lustemberg, T.-D. Nguyen-Phan, Y. Zhou, S. Luo, I. Waluyo, E. J. Crumlin, D. J. Stacchiola, J. Zhou, J. Carrasco, H. F. Busnengo, M. V. Ganduglia-Pirovano, S. D. Senanayake, J. A. Rodriguez, *Angew. Chem., Int. Ed.* **2016**, *55*, 7455.
[12] Z. Liang, T. Li, M. Kim, A. Asthagiri, J. F. Weaver, *Science* **2017**, *356*, 299.
[13] M. Ravi, M. Ranocchiari, J. A. van Bokhoven, *Angew. Chem., Int. Ed.* **2017**, *56*, 16464.
[14] G. I. Panov, V. I. Sobolev, K. A. Dubkov, V. N. Parmon, N. S. Ovanesyan, A. E. Shilov, A. A. Shteinman, *React. Kinet. Catal. Lett.* **1997**, *61*, 251.
[15] C. Hammond, N. Dimitratos, J. A. Lopez-Sanchez, R. L. Jenkins, G. Whiting, S. A. Kondrat, M. H. Ab Rahim, M. M. Forde, A. Thetford, H. Hagen, E. E. Stangland, J. M. Moulijn, S. H. Taylor, D. J. Willock, G. J. Hutchings, *ACS Catal.* **2013**, *3*, 1835.
[16] B. R. Wood, J. A. Reimer, A. T. Bell, M. T. Janicke, K. C. Ott, *J. Catal.* **2004**, *225*, 300.
[17] C. Hammond, M. M. Forde, M. H. Ab Rahim, A. Thetford, Q. He, R. L. Jenkins, N. Dimitratos, J. A. Lopez-Sanchez, N. F. Dummer, D. M. Murphy, A. F. Carley, S. H. Taylor, D. J. Willock, E. E. Stangland, J. Kang, H. Hagen, C. J. Kiely, G. J. Hutchings, *Angew. Chem., Int. Ed.* **2012**, *51*, 5129.
[18] J. Xu, R. D. Armstrong, G. Shaw, N. F. Dummer, S. J. Freakley, S. H. Taylor, G. J. Hutchings, *Catal. Today* **2016**, *270*, 93.
[19] M. H. Groothaert, P. J. Smeets, B. F. Sels, P. A. Jacobs, R. A. Schoonheydt, *J. Am. Chem. Soc.* **2005**, *127*, 1394.
[20] E. V. Starokon, M. V. Parfenov, S. S. Arzumanov, L. V. Pirutko, A. G. Stepanov, G. I. Panov, *J. Catal.* **2013**, *300*, 47.
[21] M. Ravi, V. L. Sushkevich, A. J. Knorpp, M. A. Newton, D. Palagin, A. B. Pinar, M. Ranocchiari, J. A. van Bokhoven, *Nat. Catal.* **2019**, *2*, 485.
[22] A. A. Latimer, H. Aljama, A. Kakekhani, J. S. Yoo, A. Kulkarni, C. Tsai, M. Garcia-Melchor, F. Abild-Pedersen, J. K. Nørskov, *Phys. Chem. Chem. Phys.* **2017**, *19*, 3575.
[23] J. Jang, K. Shen, C. G. Morales-Guio, *Joule* **2019**, *3*, 2589.
[24] S. Xie, S. Lin, Q. Zhang, Z. Tian, Y. Wang, *J. Energy Chem.* **2018**, *27*, 1629.
[25] X. Meng, X. Cui, N. P. Rajan, L. Yu, D. Deng, X. Bao, *Chem* **2019**, *5*, 2296.
[26] M. Stoukides, *J. Appl. Electrochem.* **1995**, *25*, 899.
[27] M. Stoukides, D. Eng, P. H. Chiang, H. Alqahtany, in *Studies in Surface Science and Catalysis*, Vol. *75*, (Eds: L. Guczi, F. Solymosi, P. TÉTÉNyi), Elsevier, New York **1993**, p. 2131.
[28] Z. W. Seh, J. Kibsgaard, C. F. Dickens, I. Chorkendorff, J. K. Nørskov, T. F. Jaramillo, *Science* **2017**, *355*, eaad4998.
[29] L. Arnarson, P. S. Schmidt, M. Pandey, A. Bagger, K. S. Thygesen, I. E. L. Stephens, J. Rossmeisl, *Phys. Chem. Chem. Phys.* **2018**, *20*, 11152.
[30] M. E. O'Reilly, R. S. Kim, S. Oh, Y. Surendranath, *ACS Cent. Sci.* **2017**, *3*, 1174.
[31] B. D. Patterson, F. Mo, A. Borgschulte, M. Hillestad, F. Joos, T. Kristiansen, S. Sunde, J. A. van Bokhoven, *Proc. Natl. Acad. Sci. U. S. A.* **2019**, *116*, 12212.
[32] A. Tomita, J. Nakajima, T. Hibino, *Angew. Chem., Int. Ed.* **2008**, *47*, 1462.
[33] B. Lee, T. Hibino, *J. Catal.* **2011**, *279*, 233.
[34] V. A. Sobyanin, V. D. Belyaev, *Solid State Ionics* **2000**, *136–137*, 747.
[35] G. L. Semin, V. D. Belyaev, A. K. Demin, V. A. Sobyanin, *Appl. Catal., A* **1999**, *181*, 131.
[36] J. O. M. Bockris, B. E. Conway, E. Yeager, R. E. White, *Comprehensive Treatise of Electrochemistry: Experimental Methods in Electrochemistry*, Plenum Press, New York **1980**.
[37] P. Promoppatum, V. Viswanathan, *ACS Sustainable Chem. Eng.* **2016**, *4*, 1736.
[38] E. E. Wolf, *Methane Conversion by Oxidative Processes: Fundamental and Engineering Aspects*, Springer, New York **1992**.
[39] A. V. de Vekki, S. T. Marakaev, *Russ. J. Appl. Chem.* **2009**, *82*, 521.
[40] K. T. Dinh, M. M. Sullivan, P. Serna, R. J. Meyer, M. Dincă, Y. Román-Leshkov, *ACS Catal.* **2018**, *8*, 8306.
[41] K. Narsimhan, K. Iyoki, K. Dinh, Y. Román-Leshkov, *ACS Cent. Sci.* **2016**, *2*, 424.
[42] R. A. Periana, D. J. Taube, S. Gamble, H. Taube, T. Satoh, H. Fujii, *Science* **1998**, *280*, 560.
[43] L. Chen, B. Yang, X. Zhang, W. Dong, K. Cao, X. Zhang, *Energy Fuels* **2006**, *20*, 915.
[44] S. Y. Chen, D. Willcox, *Ind. Eng. Chem. Res.* **1993**, *32*, 584.
[45] J. A. Labinger, J. E. Bercaw, *Nature* **2002**, *417*, 507.
[46] P. Schwach, X. Pan, X. Bao, *Chem. Rev.* **2017**, *117*, 8497.
[47] A. A. Latimer, A. R. Kulkarni, H. Aljama, J. H. Montoya, J. S. Yoo, C. Tsai, F. Abild-Pedersen, F. Studt, J. K. Nørskov, *Nat. Mater.* **2017**, *16*, 225.
[48] A. I. Olivos-Suarez, À. Szécsényi, E. J. M. Hensen, J. Ruiz-Martinez, E. A. Pidko, J. Gascon, *ACS Catal.* **2016**, *6*, 2965.
[49] S. Chempath, A. T. Bell, *J. Am. Chem. Soc.* **2006**, *128*, 4650.
[50] T. M. Gilbert, I. Hristov, T. Ziegler, *Organometallics* **2001**, *20*, 1183.
[51] I. H. Hristov, T. Ziegler, *Organometallics* **2003**, *22*, 1668.
[52] J. Haber, E. M. Serwicka, *React. Kinet. Catal. Lett.* **1987**, *35*, 369.
[53] Z. Guo, B. Liu, Q. Zhang, W. Deng, Y. Wang, Y. Yang, *Chem. Soc. Rev.* **2014**, *43*, 3480.

[54] X. Cui, H. Li, Y. Wang, Y. Hu, L. Hua, H. Li, X. Han, Q. Liu, F. Yang, L. He, X. Chen, Q. Li, J. Xiao, D. Deng, X. Bao, *Chem* **2018**, *4*, 1902.
[55] J.-F. Wu, X.-D. Gao, L.-M. Wu, W. D. Wang, S.-M. Yu, S. Bai, *ACS Catal.* **2019**, *9*, 8677.
[56] Á. Szécsényi, G. Li, J. Gascon, E. A. Pidko, *ACS Catal.* **2018**, *8*, 7961.
[57] J. Kim, M. S. Abbott, D. B. Go, J. C. Hicks, *ACS Energy Lett.* **2016**, *1*, 94.
[58] H. Stotz, L. Maier, A. Boubnov, A. T. Gremminger, J. D. Grunwaldt, O. Deutschmann, *J. Catal.* **2019**, *370*, 152.
[59] K. H. Delgado, L. Maier, S. Tischer, A. Zellner, H. Stotz, O. Deutschmann, *Catalysts* **2015**, *5*, 871.
[60] P. Lott, P. Dolcet, M. Casapu, J.-D. Grunwaldt, O. Deutschmann, *Ind. Eng. Chem. Res.* **2019**, *58*, 12561.
[61] C. R. H. de Smet, M. H. J. M. de Croon, R. J. Berger, G. B. Marin, J. C. Schouten, *Appl. Catal., A* **1999**, *187*, 33.
[62] A. B. Mhadeshwar, D. G. Vlachos, *J. Phys. Chem. B* **2005**, *109*, 16819.
[63] C. R. H. de Smet, M. H. J. M. de Croon, R. J. Berger, G. B. Marin, J. C. Schouten, *Chem. Eng. Sci.* **2001**, *56*, 4849.
[64] J. K. Nørskov, T. Bligaard, J. Rossmeisl, C. H. Christensen, *Nat. Chem.* **2009**, *1*, 37.
[65] J. Greeley, T. F. Jaramillo, J. Bonde, I. Chorkendorff, J. K. Nørskov, *Nat. Mater.* **2006**, *5*, 909.
[66] S. Wang, V. Petzold, V. Tripkovic, J. Kleis, J. G. Howalt, E. Skúlason, E. M. Fernández, B. Hvolbæk, G. Jones, A. Toftelund, H. Falsig, M. Björketun, F. Studt, F. Abild-Pedersen, J. Rossmeisl, J. K. Nørskov, T. Bligaard, *Phys. Chem. Chem. Phys.* **2011**, *13*, 20760.
[67] G. Fu, Z.-N. Chen, X. Xu, H.-L. Wan, *J. Phys. Chem. A* **2008**, *112*, 717.
[68] V. Fung, F. Polo-Garzon, Z. Wu, D.-E. Jiang, *Catal. Sci. Technol.* **2018**, *8*, 702.
[69] A. A. Latimer, A. R. Kulkarni, H. Aljama, J. H. Montoya, J. S. Yoo, C. Tsai, F. Abild-Pedersen, F. Studt, J. K. Nørskov, *Nat. Mater.* **2017**, *16*, 225.
[70] J. S. Woertink, P. J. Smeets, M. H. Groothaert, M. A. Vance, B. F. Sels, R. A. Schoonheydt, E. I. Solomon, *Proc. Natl. Acad. Sci. USA* **2009**, *106*, 18908.
[71] S. Grundner, M. A. C. Markovits, G. Li, M. Tromp, E. A. Pidko, E. J. M. Hensen, A. Jentys, M. Sanchez-Sanchez, J. A. Lercher, *Nat. Commun.* **2015**, *6*, 7546.
[72] A. S. Rosen, J. M. Notestein, R. Q. Snurr, *ACS Catal.* **2019**, *9*, 3576.
[73] Z.-J. Zhao, S. Liu, S. Zha, D. Cheng, F. Studt, G. Henkelman, J. Gong, *Nat. Rev. Mater.* **2019**, *4*, 792.
[74] W. T. Hong, M. Risch, K. A. Stoerzinger, A. Grimaud, J. Suntivich, Y. Shao-Horn, *Energy Environ. Sci.* **2015**, *8*, 1404.
[75] J. Song, C. Wei, Z.-F. Huang, C. Liu, L. Zeng, X. Wang, Z. J. Xu, *Chem. Soc. Rev.* **2020**, *49*, 2196.
[76] G. Kumar, S. L. J. Lau, M. D. Krcha, M. J. Janik, *ACS Catal.* **2016**, *6*, 1812.
[77] E. D. German, M. Sheintuch, *J. Phys. Chem. C* **2013**, *117*, 22811.
[78] J. N. Bronsted, *Chem. Rev.* **1928**, *5*, 231.
[79] M. G. Evans, M. Polanyi, *J. Chem. Soc., Faraday Trans.* **1938**, *34*, 11.
[80] T. Bligaard, J. K. Nørskov, S. Dahl, J. Matthiesen, C. H. Christensen, J. Sehested, *J. Catal.* **2004**, *224*, 206.
[81] Y. Kwon, T. Y. Kim, G. Kwon, J. Yi, H. Lee, *J. Am. Chem. Soc.* **2017**, *139*, 17694.
[82] W. Huang, S. Zhang, Y. Tang, Y. Li, L. Nguyen, Y. Li, J. Shan, D. Xiao, R. Gagne, A. I. Frenkel, F. Tao, *Angew. Chem., Int. Ed.* **2016**, *55*, 13441.
[83] O. A. Mironov, S. M. Bischof, M. M. Konnick, B. G. Hashiguchi, V. R. Ziatdinov, W. A. Goddard, M. Ahlquist, R. A. Periana, *J. Am. Chem. Soc.* **2013**, *135*, 14644.
[84] M. J. Boyd, A. A. Latimer, C. F. Dickens, A. C. Nielander, C. Hahn, J. K. Nørskov, D. C. Higgins, T. F. Jaramillo, *ACS Catal.* **2019**, *9*, 7578.
[85] L. Giordano, T. M. Østergaard, S. Muy, Y. Yu, N. Charles, S. Kim, Y. Zhang, F. Maglia, R. Jung, I. Lund, J. Rossmeisl, Y. Shao-Horn, *Chem. Mater.* **2019**, *31*, 5464.
[86] L. Giordano, P. Karayaylali, Y. Yu, Y. Katayama, F. Maglia, S. Lux, Y. Shao-Horn, *J. Phys. Chem. Lett.* **2017**, *8*, 3881.
[87] Y.-L. Lee, J. Kleis, J. Rossmeisl, Y. Shao-Horn, D. Morgan, *Energy Environ. Sci.* **2011**, *4*, 3966.
[88] C. F. Dickens, J. H. Montoya, A. R. Kulkarni, M. Bajdich, J. K. Nørskov, *Surf. Sci.* **2019**, *681*, 122.
[89] J. H. Montoya, A. D. Doyle, J. K. Nørskov, A. Vojvodic, *Phys. Chem. Chem. Phys.* **2018**, *20*, 3813.
[90] A. A. Latimer, A. Kakekhani, A. R. Kulkarni, J. K. Nørskov, *ACS Catal.* **2018**, *8*, 6894.
[91] X. Luo, Y. Li, N. K. Gupta, B. Sels, J. Ralph, L. Shuai, *Angew. Chem., Int. Ed.* **2020**, *59*, 11704.
[92] S. A. Ikbal, C. Colomban, D. Zhang, M. Delecluse, T. Brotin, V. Dufaud, J.-P. Dutasta, A. B. Sorokin, A. Martinez, *Inorg. Chem.* **2019**, *58*, 7220.
[93] A. R. Kulkarni, Z.-J. Zhao, S. Siahrostami, J. K. Nørskov, F. Studt, *Catal. Sci. Technol.* **2018**, *8*, 114.
[94] S. Sirajuddin, A. C. Rosenzweig, *Biochemistry* **2015**, *54*, 2283.
[95] M. H. Mahyuddin, A. Staykov, Y. Shiota, M. Miyanishi, K. Yoshizawa, *ACS Catal.* **2017**, *7*, 3741.
[96] J. A. Labinger, *Science* **2018**, *359*, eaar4968.
[97] K. T. Dinh, M. M. Sullivan, K. Narsimhan, P. Serna, R. J. Meyer, M. Dincă, Y. Román-Leshkov, *J. Am. Chem. Soc.* **2019**, *141*, 11641.
[98] M. Moreno-González, A. E. Palomares, M. Chiesa, M. Boronat, E. Giamello, T. Blasco, *ACS Catal.* **2017**, *7*, 3501.
[99] P. Tomkins, A. Mansouri, S. E. Bozbag, F. Krumeich, M. B. Park, E. M. C. Alayon, M. Ranocchiari, J. A. van Bokhoven, *Angew. Chem., Int. Ed.* **2016**, *55*, 5467.
[100] E. Tabor, J. Dedecek, K. Mlekodaj, Z. Sobalik, P. C. Andrikopoulos, S. Sklenak, *Sci. Adv.* **2020**, *6*, eaaz9776.
[101] A. E. Shilov, G. B. Shul'pin, *Chem. Rev.* **1997**, *97*, 2879.
[102] N. Gol'dshleger, V. Es'kova, A. Shilov, A. Shteinman, *Zh. Fiz. Khim.* **1972**, *46*, 1353.
[103] T. Zimmermann, M. Soorholtz, M. Bilke, F. Schüth, *J. Am. Chem. Soc.* **2016**, *138*, 12395.
[104] A. Sen, M. A. Benvenuto, M. Lin, A. C. Hutson, N. Basickes, *J. Am. Chem. Soc.* **1994**, *116*, 998.
[105] N. Basickes, T. E. Hogan, A. Sen, *J. Am. Chem. Soc.* **1996**, *118*, 13111.
[106] R. Palkovits, M. Antonietti, P. Kuhn, A. Thomas, F. Schüth, *Angew. Chem., Int. Ed.* **2009**, *48*, 6909.
[107] M. Lyubovsky, L. Pfefferle, *Catal. Today* **1999**, *47*, 29.
[108] A. D. Mayernick, M. J. Janik, *J. Catal.* **2011**, *278*, 16.
[109] M. H. Ab Rahim, M. M. Forde, R. L. Jenkins, C. Hammond, Q. He, N. Dimitratos, J. A. Lopez-Sanchez, A. F. Carley, S. H. Taylor, D. J. Willock, D. M. Murphy, C. J. Kiely, G. J. Hutchings, *Angew. Chem., Int. Ed.* **2013**, *52*, 1280.
[110] N. Agarwal, S. J. Freakley, R. U. McVicker, S. M. Althahban, N. Dimitratos, Q. He, D. J. Morgan, R. L. Jenkins, D. J. Willock, S. H. Taylor, C. J. Kiely, G. J. Hutchings, *Science* **2017**, *358*, 223.
[111] R. S. Rocha, R. M. Reis, M. R. V. Lanza, R. Bertazzoli, *Electrochim. Acta* **2013**, *87*, 606.
[112] J. Qiao, S. Tang, Y. Tian, S. Shuang, C. Dong, M. M. F. Choi, *Sens. Actuators, B* **2009**, *138*, 402.
[113] N. Spinner, W. E. Mustain, *J. Electrochem. Soc.* **2012**, *159*, E187.
[114] N. Spinner, W. E. Mustain, *J. Electrochem. Soc.* **2013**, *160*, F1275.
[115] M. Ma, B. J. Jin, P. Li, M. S. Jung, J. I. Kim, Y. Cho, S. Kim, J. H. Moon, J. H. Park, *Adv. Sci.* **2017**, *4*, 1700379.
[116] R. Palkovits, C. von Malotki, M. Baumgarten, K. Müllen, C. Baltes, M. Antonietti, P. Kuhn, J. Weber, A. Thomas, F. Schüth, *ChemSusChem* **2010**, *3*, 277.
[117] S. F. Liu, F. Nusrat, *Mol. Catal.* **2019**, *463*, 16.
[118] R. S. Kim, Y. Surendranath, *ACS Cent. Sci.* **2019**, *5*, 1179.
[119] K. W. Frese, *Langmuir* **1991**, *7*, 13.
[120] J. S. Jirkovský, I. Panas, E. Ahlberg, M. Halasa, S. Romani, D. J. Schiffrin, *J. Am. Chem. Soc.* **2011**, *133*, 19432.
[121] R. B. Rankin, J. Greeley, *ACS Catal.* **2012**, *2*, 2664.
[122] T. R. Baldwin, R. Burch, *Appl. Catal.* **1990**, *66*, 359.

[123] M. Joglekar, V. Nguyen, S. Pylypenko, C. Ngo, Q. Li, M. E. O'Reilly, T. S. Gray, W. A. Hubbard, T. B. Gunnoe, A. M. Herring, B. G. Trewyn, *J. Am. Chem. Soc.* **2016**, *138*, 116.
[124] J. Deng, S.-C. Lin, J. Fuller, J. A. Iñiguez, D. Xiang, D. Yang, G. Chan, H. M. Chen, A. N. Alexandrova, C. Liu, *Nat. Commun.* **2020**, *11*, 3686.
[125] C. E. Thomas, B. D. James, F. D. Lomax, I. F. Kuhn, *Int. J. Hydrogen Energy* **2000**, *25*, 551.
[126] J. Peischl, T. B. Ryerson, K. C. Aikin, J. A. de Gouw, J. B. Gilman, J. S. Holloway, B. M. Lerner, R. Nadkarni, J. A. Neuman, J. B. Nowak, M. Trainer, C. Warneke, D. D. Parrish, *J. Geophys. Res.: Atmos.* **2015**, *120*, 2119.
[127] B. Huang, S. Muy, S. Feng, Y. Katayama, Y.-C. Lu, G. Chen, Y. Shao-Horn, *Phys. Chem. Chem. Phys.* **2018**, *20*, 15680.
[128] O. M. Magnussen, A. Groß, *J. Am. Chem. Soc.* **2019**, *141*, 4777.
[129] F. Bacon, *Ind. Eng. Chem. Res.* **1960**, *52*, 301.

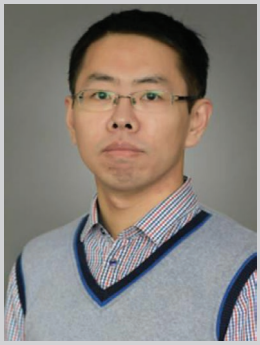

Shuai Yuan received his B.Sc. in Chemistry from Shandong University in 2013. He then went to Texas A&M University, and received his Ph.D. in Chemistry in 2018 working under the supervision of Prof. Hong-Cai Zhou. His graduate research is focused on the synthesis and functionalization of stable metal–organic frameworks (MOFs) for energy conversion and storage. He joined the Electrochemical Energy Laboratory and the Román Group at MIT in September 2019 as a post-doctoral researcher. His research at MIT is to explore the application of MOFs for heterogenous electrocatalysis.

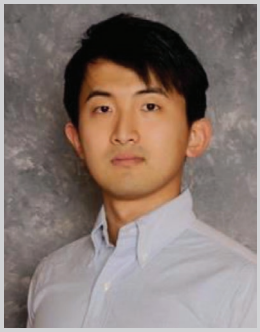

Yanding Li obtained his M.S. from the University of Tokyo in 2015. He then received his Ph.D. in 2019 from the University of Wisconsin-Madison (USA) under the supervision of Prof. John Ralph on Plant Science and Prof. James A. Dumesic on Catalytic Biomass Conversion. He is currently a postdoctoral fellow in Prof. Yuriy Román's group at Massachusetts Institute of Technology. His research interests include kinetic studies of lignin hydrogenolysis process and biomass upgrading by electrocatalysis.

Yuriy Román-Leshkov is from Mexico City, Mexico. He earned his B.S.E. in Chemical Engineering from the University of Pennsylvania in 2002, and Ph.D. in Chemical and Biological Engineering from the University of Wisconsin-Madison in 2008 working under the supervision of Prof. James A. Dumesic. He then moved to the California Institute of Technology to do postdoctoral research in the synthesis and characterization of microporous and mesoporous materials in the group of Prof. Mark E. Davis. His research group at MIT focuses on designing heterogenous catalysts based on porous materials, and their applications in energy, biomass conversion, biofuels, and CO_2 utilization.

Yang Shao-Horn is the W.M. Keck professor of Energy at the Massachusetts Institute of Technology (MIT) as well as a professor of Mechanical Engineering and Materials Science and Engineering. Her interests include surface science, catalysis/electrocatalysis, and design of electron and phonon structures of materials for electrochemical energy storage, solid-state ionics, photoelectrochemical conversion, and clean environmental applications.